Analyses of Monthly Mean Cloudiness and Their Influence Upon Model-Diagnosed Radiative Fluxes

CHARLES T. GORDON, RUSSELL D. HOVANEC, AND WILLIAM F. STERN

Geophysical Fluid Dynamics Laboratory/NOAA, Princeton University

Two different monthly mean analyses of low, middle, and high cloud amounts for January 1977 and July 1979 are compared: 3DNEPH is a condensed version (northern hemisphere only) of the Air Force 3D-Neph analysis, which incorporates satellite data plus surface observations of clouds and auxiliary meteorological data. SFCOBS is objectively analyzed from surface observations of clouds. The SFCOBS and 3DNEPH analyses of low cloud amounts agree qualitatively in the winter extratropics. The 3DNEPH ITCZ is much more sharply defined than the SFCOBS. The sensitivity of radiative fluxes to 3DNEPH, SFCOBS, and zonal mean 3DNEPH clouds is then evaluated. The fluxes are diagnosed by a cloud-radiation model utilizing "observed" monthly mean temperature and water vapor fields and are verified against satellite data. The outgoing longwave radiative flux clearly verifies best for 3DNEPH clouds and worst for zonal mean 3DNEPH clouds in the tropics. It is predominantly controlled by surface temperature in the winter extratropics. Generally speaking, the shortwave fluxes do not verify as well as the longwave fluxes. Also, outside of the winter extratropics, the net radiative fluxes correlate poorly with observation. Biases in the zonal mean long and shortwave fluxes can be reduced by adjusting other cloud-related parameters. Based upon the above results, it may be worthwhile to construct a monthly mean cloud climatology from a condensed version of the 3D-Neph. However, alternative strategies should also be explored, such as the development of cloud analysis schemes that constrain the model-diagnosed net radiative flux to be consistent with observation.

1. INTRODUCTION

The sensitivity of the atmospheric radiative balance to clouds and its implications for climate have been widely investigated during the past decade. For example, the relative importance of the albedo vs. the greenhouse effect of clouds has been addressed by Schneider [1972], Cess [1976], Ohring and Clapp [1980], Hartmann and Short [1980], Stephens and Webster [1981], Cess et al. [1982], and others. In turn the specification of improved monthly mean cloud climatologies in general circulation models (GCM's) may affect the results of climate sensitivity experiments and/or the time mean predictive capability of GCM's over the 1-month range and beyond.

Several cloud parameters presumably affect the atmospheric radiative balance, as suggested in the Report of the Study Conference on Parameterizations of Extended Cloudiness and Radiation for Climate Models [JOC, 1978]. Among them, cloud amount is widely used in present generation GCM cloud-radiative parameterizations. As Stephens and Webster [1979] have shown the net radiative flux at the top of the atmosphere is indeed sensitive, in the tropics, to longitudinal variations of cloud amount. However, in their experiments the domain was confined to a strip of longitude at latitude 25°N, and the longitudinal variation of cloud amount was idealized. In principle, similar sensitivity experiments could be performed over a more extensive domain, using a more realistic, geographically varying specification of cloud amount. But to our knowledge the available cloud amount climatologies are limited to total cloud amount [Landsberg, 1945; Clapp, 1964; Berlyand and Strokina, 1974], to zonal means [Telegadas and London, 1954], or to oceanic domains [Sadler et al., 1976]. On the other hand the construction of more suitable cloud climatologies, would require a vast amount of data processing. In any case, idealized temperature and water vapor profiles are

usually specified in diagnostic cloud-radiation sensitivity studies.

Given the above circumstances, a logical next step would be to calculate radiative fluxes for geographically varying, observed monthly mean fields of cloud amount, temperature, and water vapor for a couple of specific months. The results could provide guidance for the construction of improved monthly mean cloud climatologies. Pursuant to this objective, the present investigation addresses three main topics:

1. Two hemispheric, monthly mean analyses of low, middle, and high cloud amounts for January 1977 and July 1977 are intercompared. These analyses—3DNEPH and SFCOBS—are constructed from quasi-independent data sources.

2. The sensitivity of radiative fluxes, mainly at the top of the atmosphere, to the 3DNEPH and SFCOBS as well as zonal mean 3DNEPH analyses of cloud amount is calculated by an established cloud-radiation model, given "observed" monthly mean fields of temperature and water vapor. The fluxes are validated against satellite scanning radiometer data.

3. The sensitivity of radiative fluxes to variations in other radiative parameters, i.e., emissivity and cloud top height of high clouds, cloud albedos, and snow cover, is examined. These latter calculations provide some indication of the relative importance of cloud amount vs. other radiative parameters for the radiation balance as well as a check of the cloud-radiation parameterizations of a typical present-generation GCM.

Ideally, the longitudinal variation of cloud parameters such as cloud top height, cloud base, cloud type, reflectivity, and emissivity should be taken into account [JOC, 1978], where the latter two parameters may be expressed in terms of the ice or liquid water path length [Stephens and Webster, 1981]. In the present study, however, all cloud parameters other than cloud amount will correspond to global or zonal mean climatological specifications (see Table 1, Figure 1, and section 4) currently used in extended range prediction models at the Geophysical Fluid Dynamics Laboratory (GFDL). This ap-

TABLE　　Cloud Albedos, Reflectivities, and Absorptivities

Case	Cloud Parameter	High Clouds	Middle Clouds	Low Clouds
January 1977	Albedo (standard)	0.21	0.48	0.69
	Absorptivity (standard)	0.005	0.020	0.035
July 1979	Albedo (standard)	$0.241-0.0677 \cos Z$	$0.521-0.1548 \cos Z$	$0.673-0.2225 \cos Z$
	Absorptivity (standard)	0.005	0.020	0.035
January 1977	Albedo (optional)	0.21	0.45	0.57
January 1977		$0.241-0.0677 \cos Z$	$0.521-0.1548 \cos Z$	$0.673-0.225 \cos Z$
January 1977	Reflectivity (optional)	$0.21, \lambda < 0.7 \ \mu m$	$0.45, \lambda < 0.7 \ \mu m$	$0.57, \lambda < 0.7 \ \mu m$
		$0.19, \lambda > 0.7 \ \mu m$	$0.35, \lambda > 0.7 \ \mu m$	$0.47, \lambda > 0.7 \ \mu m$
January/July		$0.248-0.0820 \cos Z, \lambda < 0.7 \ \mu m$	$0.531-0.1757 \cos Z, \lambda < 0.7 \ \mu m$	$0.673-0.2225 \cos Z, \lambda < 0.7 \ \mu m$
		$0.232-0.0900 \cos Z, \lambda > 0.7 \ \mu m$	$0.427-0.1657 \cos Z, \lambda > 0.7 \ \mu m$	$0.573-0.2225 \cos Z, \lambda > 0.7 \ \mu m$
January 1977	Absorptivity (optional)	0.020	0.150	0.150

proach seems prudent, considering the type of data available to us and the limited vertical resolution (nine sigma levels) of our GCM. Eventually, global analyses of cloud parameters explicitly related to microphysical properties of real clouds may become available.

Incidentally, we shall loosely define "cloud amount" as the fraction of sky covered by low, middle, and/or high clouds. Some ambiguity arises, however, because satellite measurements are relevant to areal cloud amount, whereas surface observers make point observations of cloud amount. Also,

satellite observations and surface observations are affected by different biases, as discussed by *Hoyt* [1977]. Our strategy is simply to compare the 3DNEPH and SFCOBS analyses at face value after discarding internally inconsistent data. The relevant cloud level(s) will be indicated by the adjectives "low," "middle," "high," "total," or "layered." Here, "total" cloud amount will refer to the fraction of sky covered by all clouds irrespective of layer, whereas "layered cloud amounts" will refer collectively to the low, middle, and high cloud amounts. In addition, the terms "cloud cover," "fractional cloud
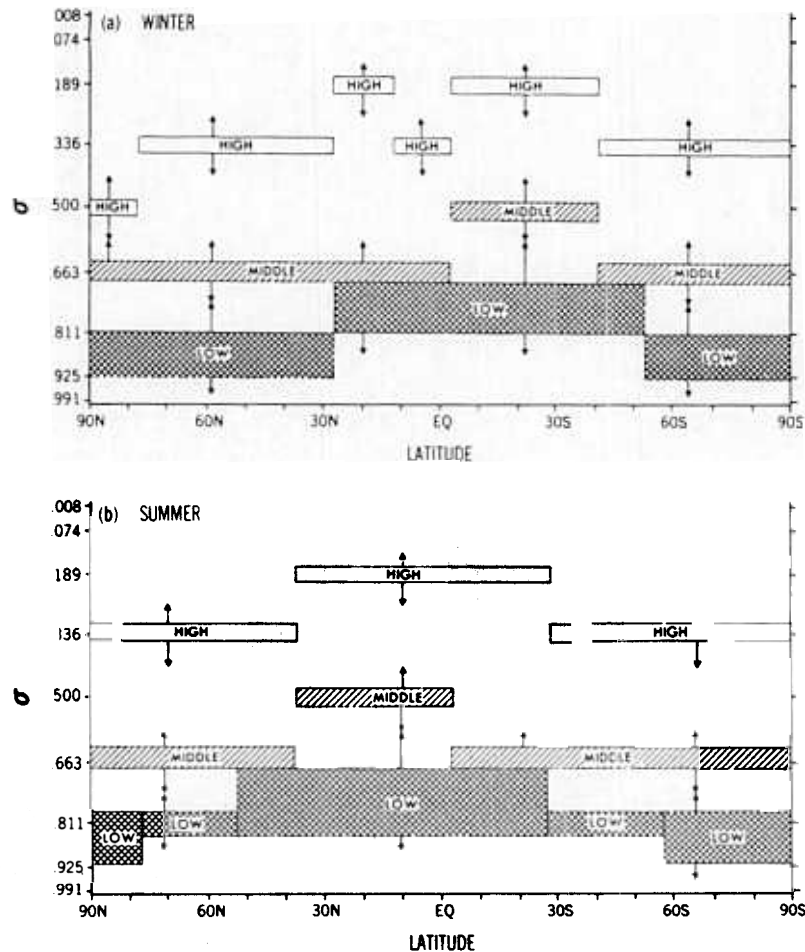

Fig. 1.　Schematic diagram of the vertical placement of the clouds used in the standard radiative flux calculations: (top) winter climatology, (bottom) summer climatology, σ is the vertical coordinate.

amount," and "cloudiness" will be used interchangeably with "cloud amount."

2. THE CLOUD DATA SETS AND ANALYSES OF CLOUD AMOUNT

The 3DNEPH and SFCOBS monthly mean analyses of low, middle, and high cloud amounts have been constructed from the U.S. Air Force Global Weather Central (AFGWC) 3D-Neph cloud analysis and surface-based observations of clouds, respectively. The AFGWC 3D-Neph analysis is based primarily upon satellite-derived visible and longwave flux data supplemented by surface-based observations of clouds and auxilliary weather information. The SFCOBS analysis is based exclusively upon surface level 2 data, i.e., station data. Another analysis, i.e., MELESHKO, which is obtained by using the scheme of *Meleshko and Wetherald* [1981], is briefly discussed in Appendix A.

It was feasible to process cloud data for only one summer month (July 1979) and one winter month (January 1977). In fact the 3D-Neph processing was restricted to the northern hemisphere. July 1979 falls within the period of the First GARP Global Experiment (FGGE), when analyses of meteorological variables are apt to be particularly good; January 1977 is notable for its persistent Pacific North-American block, which was successfully simulated by *Miyakoda et al.* [1983].

The construction of the 3DNEPH and SFCOBS analyses is now described in some detail.

3DNEPH

The AFGWC 3D-Neph analysis, which serves as the input, is probably the most comprehensive global cloud data set currently available [*Henderson-Sellers et al.*, 1981]. A documentation of the AFGWC analysis procedures as well as a chronology of improvements may be found in *Fye* [1978].

The huge volume of 3D-Neph data has intimidated potential users in the fields of climate modeling and cloud climatology. According to the available format, i.e., the box-time file, each hemisphere is subdivided into 60 boxes. The global analysis for a particular month spans 120 tapes, i.e., one tape per box per month. Each box contains a 64 × 64 grid (4096 points) whose average grid spacing is 25 nautical miles (slightly less than 50 km). The temporal resolution is nominally 3 hours. Twenty-two cloud-related variables are archived, i.e., total cloud cover; cloud amounts at 15 atmospheric levels; the heights of the lowest cloud base and highest cloud top; types of low, middle, and high clouds; and significant weather.

The AFGWC 3D-Neph analysis incorporates both satellite and "conventional" observations. Satellite data is usually obtained from two Military Defense Satellite Program (DMSP) polar orbiters alone, while National Oceanographic and Atmospheric Administration (NOAA) satellites provide a backup capability. In practice, data from the NOAA 5 satellite was utilized during January 1977 but not during July 1979. The DMSP satellites feature high-resolution sensors for the 0.4–1.0 μm visible and 10.2–12.8 μm infrared bands and provide complete equatorial coverage, roughly every 6 hours. The total cloud cover N_T is estimated separately by the visible and infrared satellite data processors by means of threshold techniques, and the greater of the two estimates is retained. The infrared data processor identifies up to two cloudy layers or one partly cloudy layer and the corresponding cloud top height. In the conventional data processor, surface observations take precedence over aircraft reports and radiosonde


```
Input:  60 tapes (NH) for January 1977

        1 3D-Neph box per tape.
        15 levels + total 3D-Neph cloud amount and
        auxilliary information.                        per box
        3 hour sampling interval.
```

```
Interpolate 15 levels + total 3D-Neph cloud
amount + auxilliary information to 16x16         per box
grid points.
Compute daily means and monthly mean.
```

```
Interpolate data from coarse mesh boxes to
northern hemisphere portion of a 54x64
Gaussian latitude-longitude grid.
Reduce 15 levels of cloud amounts to three
layers, i.e., low, middle and high.
Normalize the layered amounts to be con-
sistent with the AFGWC 3D-Neph total cloud
amount.
```
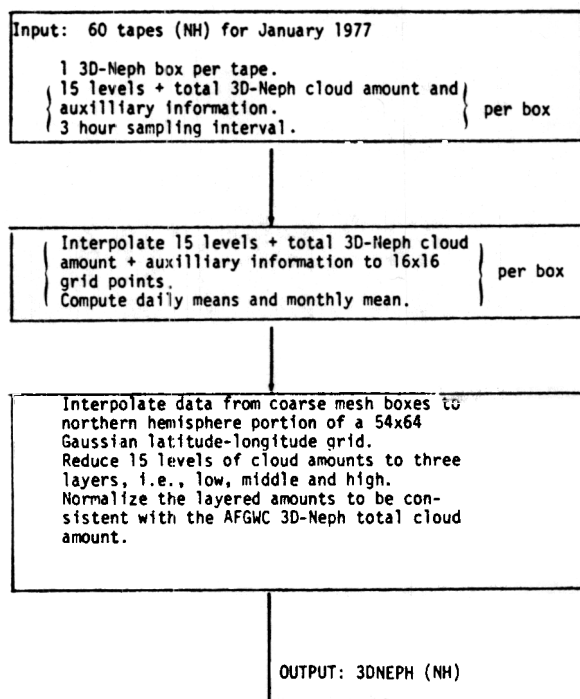
```
OUTPUT: 3DNEPH (NH)
```

Fig. 2. Flow chart illustrating the reconstruction of the final 3DNEPH cloud analysis from the AFGWC 3D-Neph.

observations. The satellite-derived and conventional data are merged by a decision tree processor, which selects the higher of the two estimates of total cloud cover if $N_T < 0.55$ and the satellite estimate if $N_T > 0.55$. Thus a positive bias may be introduced into the analysis. Consistency checks are made, and a quality control log is available for post-1976 data sets.

Various objections may be expressed about the 3D-Neph analysis procedures. One fear is that it contains bogus cloud amounts derived from radiosonde observations and an empirical cloudiness-relative humidity relationship. But about 75% of the 3D-Neph analysis is supposed to be satellite-derived. Furthermore, since the most timely data takes precedence, satellite data should prevail in the tropical and even extratropical oceans, where conventional data are sparse.

Second, the hybrid nature of the 3D-Neph analysis eliminates the possibility of a truly independent verification. But there is a tradeoff, i.e., for low clouds the overall quality of the 3D-Neph analysis may be improved by the inclusion of surface observations.

Third, the volume of 3D-Neph data is unnecessarily large. For example the 50-km horizontal resolution is too fine for most GCM applications. Moreover, cloud amounts of distinct cloud layers have been interpolated, subject to assumptions about cloud layer thickness, to 15 predetermined atmospheric levels. Fortunately, in the future, cloud amounts for distinct cloud layers will be archived instead.

Fourth, apparent diurnal cycles in 3D-Neph analyses over the oceans may be erroneous [*Warren et al.*, 1981]. Also, climatological statistics of cloud amount may be affected by modifications in satellite instrumentation and 3D-Neph analysis procedures or malfunctions of the DMSP satellites.

The reconstruction of the 3D-Neph analysis is shown schematically in Figure 2. The data is drastically compressed so as to span only a fraction of a tape. The process involves a few horizontal interpolations to coarser grids, time averaging, and elimination of some 3D-Neph variables. The final data set

contains daily mean and monthly mean hemispheric fields of low (n_l), middle (n_m), high (n_h), and total (N_T) cloud amount on the transform grid of a rhomboidally truncated spectral GCM. The grid has 64 equispaced longitudes and 54 almost equispaced Gaussian latitudes.

Layered cloud amounts are obtained at each grid point as follows. Each of the 15 3D-Neph levels is designated as a low, middle, or high level, according to the climatological designation of the nearest vertical level of the GCM (Figure 1). Preliminary estimates of high, middle, and low cloud amounts are given by the respective maxima from high-, middle-, and low-designated 3D-Neph levels. A preliminary total cloud cover field is computed under the assumption that clouds from different layers randomly overlap. Finally, the preliminary estimates are normalized such that the computed total agrees with the reported 3D-Neph total to within 2% whenever possible. The rationale is that the 3D-Neph total is believed to be more reliable than the individual 3D-Neph layered amounts. In this first attempt, auxiliary 3D-Neph information such as cloud type and "significant weather" have been ignored. The order of horizontal, vertical, and time averaging did not appear to significantly affect the final monthly mean analyses.

SFCOBS

Surface-based observations of clouds are included in the National Center for Atmospheric Research's (NCAR) archive of three-hourly surface data. The data network encompasses land stations as well as ship reports transmitted via the global communications satellite network. It excludes delayed ship log reports that could augment the oceanic data base of clouds by up to 35%. The cloud information is contained in the sky cover group and the cloud cover group $n_{l,m}C_lB_{l,m}C_mC_h$ of the surface synoptic reports. If low clouds are present, $n_{l,m}$ is the fractional amount of all the genera of low clouds, i.e., $n_{l,m} = n_l$; if low clouds are not present but middle clouds are, then $n_{l,m} = n_m$. The symbols C_l, C_m, and C_h correspond to dominant low, middle, and high cloud types, whereas $B_{l,m}$ is the base of the lowest low or middle layer cloud. The SFCOBS scheme categorizes cumulus or cumulonimbus as low clouds. The number of cloud layers can be deduced from C_l, C_m, and C_h. The cloud-type information is used for no other purpose. If there is only one cloud layer, then $n_{l,m}$ should equal N_T. If there are two layers, the fractional amounts can be deduced from $n_{l,m}$ and N_T, assuming random overlap. Then using a similar procedure as in Telegadas and London [1954], $n_m = (N_T - n_l)/(1 - n_l)$, or $n_h = (N_T - n_l)/(1 - n_l)$, or $n_h = (N_T - n_m)/(1 - n_m)$. If low, middle, and high layers are reported simultaneously, the information is insufficient to determine the layered cloud amounts, and the data are discarded. This occurred at fewer than 5% of the stations. Other causes of data rejection were incomplete or missing cloud groups, missing sky cover, or an inconsistency between $n_{l,m}$ and N_T (e.g., $n_{l,m} \neq N_T$ when one cloud layer was reported or $n_{l,m} > N_T$ when two layers were reported).

After checking the cloud data, daily means of low, middle, and high cloud amounts were computed at each station. Then, monthly means were computed for each $1° \times 1°$ square on a regular latitude-longitude grid. In this calculation, all daily mean station values within the grid square were given equal weight. Next, the objective analysis scheme of Levitus and Oort [1977] was applied to n_l, n_m, n_h, and N_T. To make fuller use of the data, the radius of influence was decremented on three successive passes from 1600 km to 800 km to 400 km. Squares

without station data were not permitted to influence any other squares on any pass. The first guess fields at such squares on the first pass were based upon the Telegadas and London [1954] zonal mean northern hemisphere climatology and the Sasamori et al. [1972] southern hemisphere climatology for n_l, n_m, n_h, and N_T. Meanwhile, the results of the first and second passes provided the first guess fields on the second and third passes, respectively. Finally, the objective analyses of n_l, n_m, n_h, and N_T were interpolated from the $1° \times 1°$ grid to the much coarser GCM grid.

The surface data coverage is illustrated in Figure 3. Each dot in Figure 3a signifies that usable cloud observations were reported within the relevant $1° \times 1°$ grid square on at least one day during January 1977. The major shipping lanes are easily identifiable. But few observations are found south of 30°S or 40°S. Actually, Figure 3a gives an overly optimistic impression of the data density over the tropical and even extratropical oceans. In fact, as illustrated in Figure 3b, substantially fewer oceanic grid squares contained observations on a typical day.

The SFCOBS analysis of monthly mean cloud amount has at least three limitations. The scarcity of oceanic cloud observations during a specific month is most serious, especially where synoptic day-to-day variability is locally large. According to Warren et al. [1981], about 150 independent observations per 90 days are necessary to adequately represent the seasonal mean for a particular $5° \times 5°$ box. Second, surface observers tend to underestimate the amount of high clouds [Telegadas and London, 1954] and overestimate the amount of low clouds. Third, the scheme cannot adequately represent the existence of three distinct layers of cloud or deep convective clouds with high, cold tops.

3. COMPARISON OF THE CLOUD ANALYSES

In this section the 3DNEPH vs. SFCOBS monthly mean analyses of cloud amounts for January 1977 and July 1979 are compared. For this purpose, latitude-longitude maps of cloud amount fields, as well as latitudinal profiles of zonal mean cloud amounts and of the longitudinal correlation between 3DNEPH vs. SFCOBS analyses, are presented. Maps of monthly mean 3DNEPH and SFCOBS low, high, and total cloud amounts are shown in Figures 4 and 5. The domain for SFCOBS is 90°N to 30°S, since very few surface-based observations of cloudiness were available poleward of 30°S; and the 3DNEPH analysis extends only to the equator. For a comparison with a climatology of total cloud amount the reader may refer to Berlyand and Strokina [1974].

The January 1977 monthly mean 3DNEPH and SFCOBS low cloud amounts, i.e., n_l (Figure 4a) agree qualitatively in the northern hemisphere mid-latitudes, where the 3DNEPH utilizes many surface observations. But SFCOBS displays more dramatic land-sea contrast. Meanwhile, the January 1977 3DNEPH and SFCOBS high cloud amounts n_h (Figure 4b) exhibit large systematic differences over the mid-latitude oceans and some continental regions. In the vicinity of latitude 15°N the SFCOBS n_l field reveals a less extreme minimum than the 3DNEPH.

South of the equator, the 3DNEPH has not been reconstructed. But the SFCOBS analyses of n_l (Figure 4a) and n_h (Figure 4b) lack a well-defined cloud band over the south tropical Pacific Ocean. Similarly, n_h lacks intense maxima over Brazil and south equatorial Africa. These apparent deficiencies are somewhat less pronounced in the SFCOBS analysis of

≥1 CLOUD OBS.   JAN 1-31, 1977

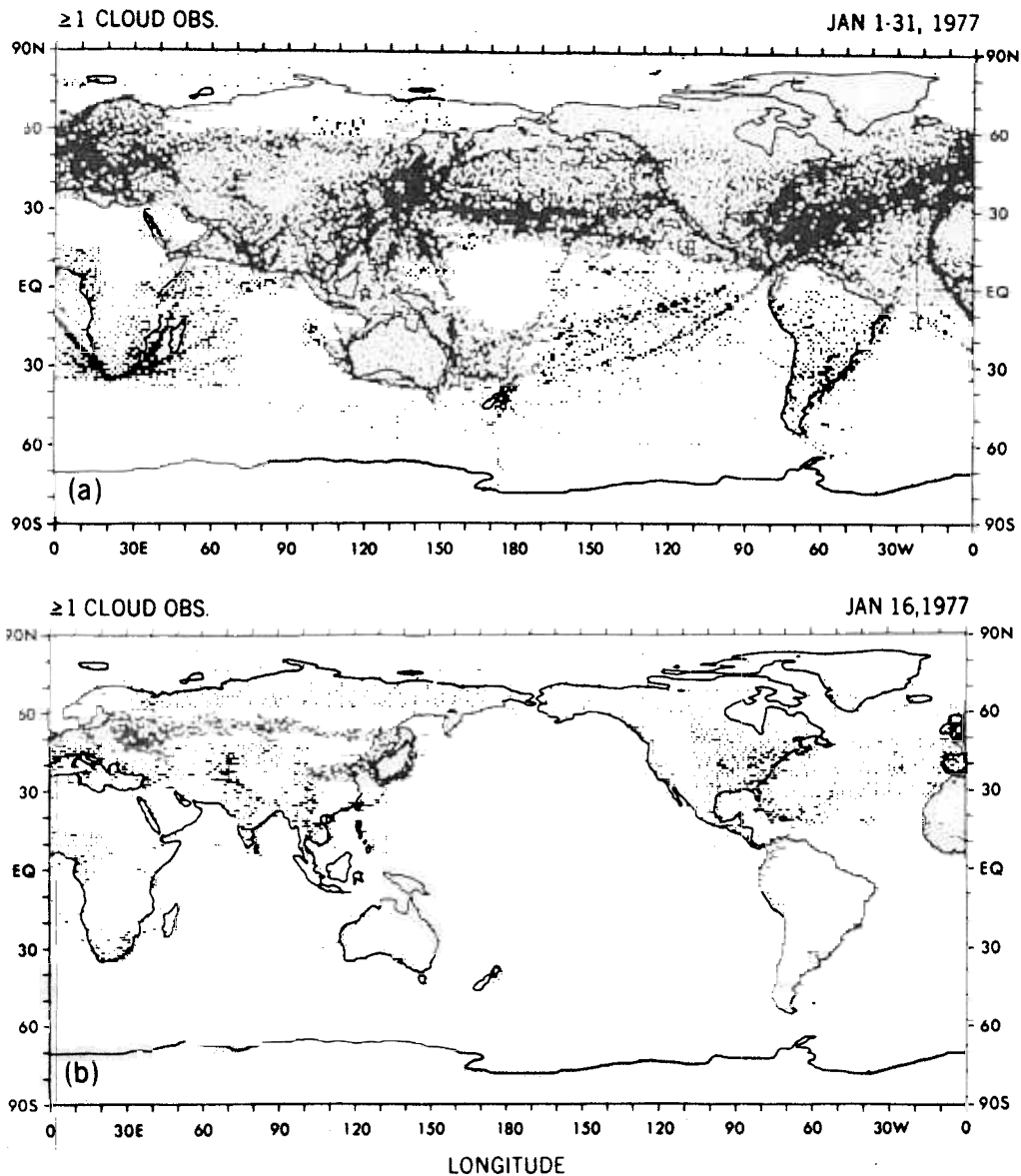≥1 CLOUD OBS.   JAN 16,1977

LONGITUDE

Fig. 3. Distribution of surface-based observations of cloud amount over the 90°N–90°S domain. One or more usable cloud observations were available within each 1° × 1° grid square containing a dot on (a) at least one day during January 1977 and on (b) January 16, 1977.

middle cloudiness (not shown). Perhaps the above results can be partially attributed to insufficient tropical oceanic data and the tendency of surface observers to underestimate amounts and/or heights of high clouds.

Each total cloud amount field N_T (Figure 4c) incorporates the characteristics, including systematic biases, of the corresponding low and, to a lesser extent, high cloud amount field.

During July 1979 (Figure 5a), maxima of SFCOBS low cloud amounts in the Pacific and Atlantic are located northward and eastward, respectively, of their January 1977 position. Also, the correspondence between 3DNEPH and SFCOBS n_l is now poorer in the central North Pacific and eastern Atlantic. Perhaps sporadic ship observations are less representative of the monthly mean when the extratropical circulation is dominated more by transients (July 1979) than by quasi-stationary disturbances (January 1977). The discrepancy between the 3DNEPH vs. SFCOBS high cloudiness at mid-latitudes is less pronounced during July 1979 (Figure 5b) than during January 1977.

In the tropics the July 1979 3DNEPH analysis of N_T (Figure 5c), n_l, and n_h is suggestive of an intense ITCZ centered near 8°N. In comparison the SFCOBS ITCZ is poorly defined, except over Africa and the Bay of Bengal. However, in the regions of stratocumulus formation off the west coasts of South and Central America and southern Africa the SFCOBS analysis indicates low cloudiness.

The 3DNEPH and SFCOBS analyses of n_l and n_h have been cross correlated at each latitude after subtracting the appropriate zonal mean values. For example the correlation coefficient between the SFCOBS and 3DNEPH analyses of n_l is defined as

r_{n_l}(SFCOBS, 3DNEPH)

$$= \frac{\langle n_l'(\text{SFCOBS}) n_l'(\text{3DNEPH})\rangle}{[\langle n_l'^2(\text{SFCOBS})\rangle]^{1/2}[\langle n_l'^2(\text{3DNEPH})\rangle]^{1/2}} \quad (1)$$

Here, angle brackets denote zonal means and primes denote the departure from the zonal mean. Latitudinal profiles of r_{n_l}
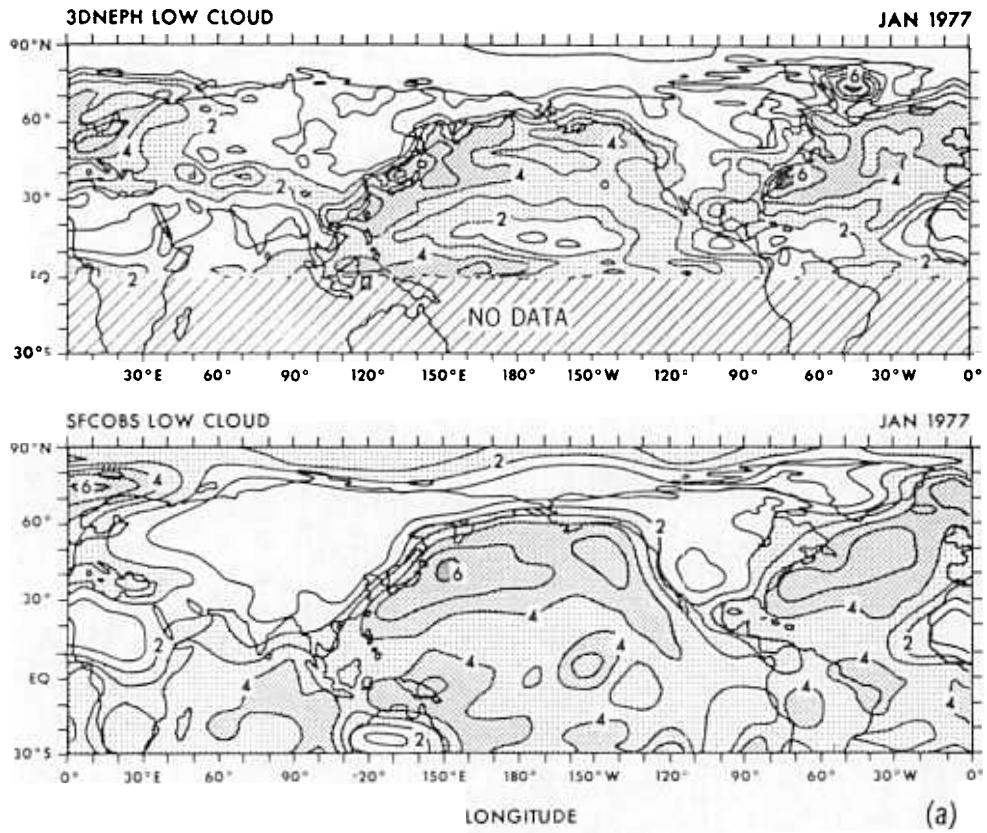
3DNEPH LOW CLOUD   JAN 1977

SFCOBS LOW CLOUD   JAN 1977

LONGITUDE

(a)

Fig 4a

3DNEPH HIGH CLOUD   JAN 1977

SFCOBS HIGH CLOUD   JAN 1977

LONGITUDE

(b)
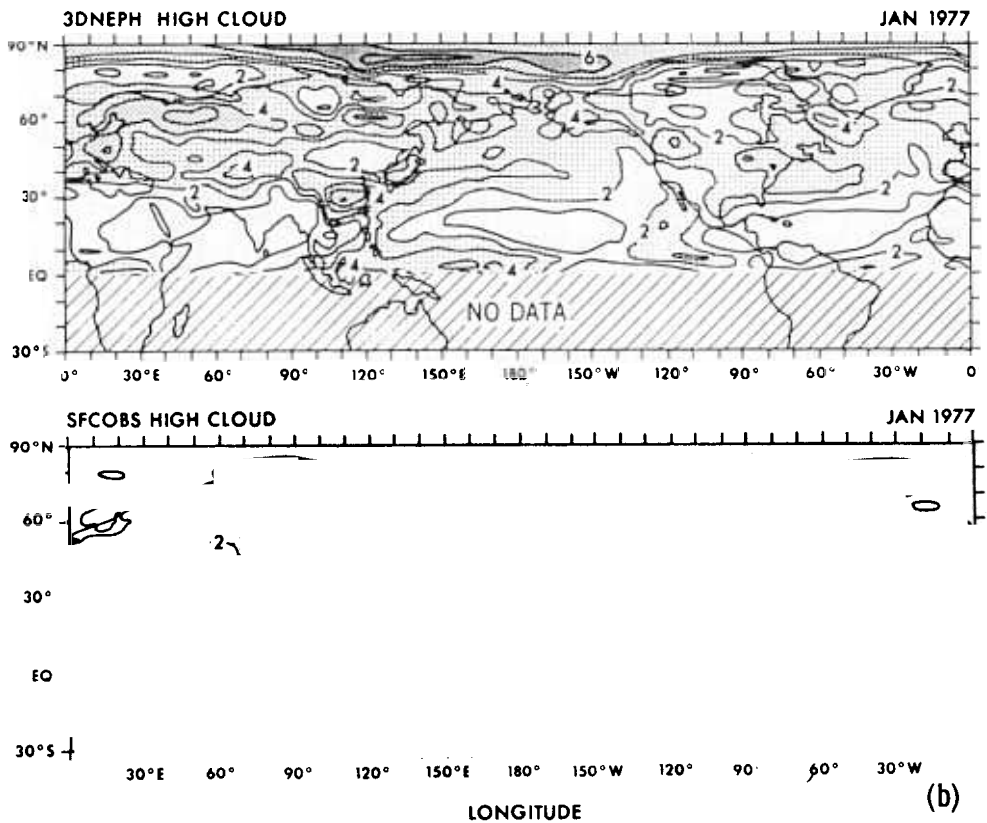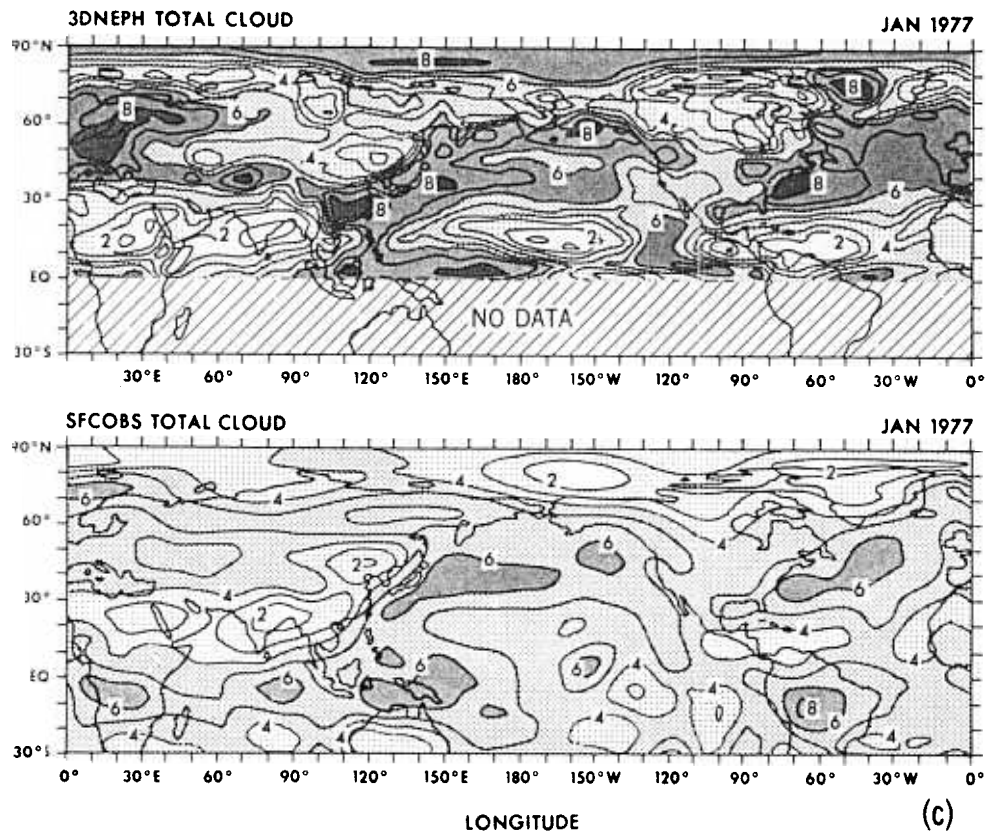
Fig 4b

Fig. 4. Monthly mean 3DNEPH and SFCOBS analyses of cloud amount for January 1977 over the 90°N–30°S domain: (a) low clouds, (b) high clouds, (c) total clouds. Contour interval = 0.1. Intensity of stippling increases with cloud amount.

and r_{n_h} (Figure 6) provide a quantitative measure of comparison of the two cloud analyses.

The results tend to confirm what was already visually apparent. In January 1977, SFCOBS and 3DNEPH low cloud amounts are moderately well correlated, unlike the corresponding high cloud amounts. However, in July 1979 the correlation between SFCOBS vs. 3DNEPH high cloud amounts improves considerably within the 20°N–50°N latitude belt.

Latitudinal profiles of observed zonal mean cloud amounts for January 1977 (Figure 7) and July 1979 (Figure 8) illustrate various systematic differences between analyses. "LONDON" denotes a zonal mean climatology of cloud amount based upon Telegadus and London [1954] in the northern hemisphere and Sasamori et al. [1972] in the southern hemisphere. The corresponding northern hemisphere, southern hemisphere, and global means have been tabulated in Table 2.

Within the 30°N–70°N extratropical belt, the 3DNEPH and SFCOBS profiles of n_l agree qualitatively, whereas the discrepancy between SFCOBS and LONDON climatology is quite large. At north polar latitudes the 3DNEPH analysis apparently underestimates the low cloudiness during July 1979.

In the northern hemisphere tropics there is somewhat more SFCOBS low cloudiness than 3DNEPH during January 1977. Conversely, there is substantially more 3DNEPH low cloudiness than SFCOBS during July 1979. But the July 1979 SFCOBS ITCZ maximum in n_l is still sharper than LONDON. This latter results may be due to an enhancement of the surface network since 1954 as well as natural variability.

A long record apparently does not compensate for the lack of ship reports at key locations.

As for high cloudiness n_h there is more 3DNEPH than SFCOBS in the northern hemisphere extratropics during January 1977 as well as July 1979. Also, the July 1979 3DNEPH analysis reveals a much sharper ITCZ than SFCOBS. Similarly, the 3DNEPH total cloudiness is substantially greater then SFCOBS in the July 1979 ITCZ region. An intrinsic positive bias in the AFGWC 3D-Neph analysis and a lack of surface data over vast oceanic regions may be among the contributing factors.

4. CALCULATION OF MODEL-DIAGNOSED RADIATIVE FLUXES

The focus now shifts to "model-diagnosed" longwave, shortwave, and net radiative fluxes at the top of the atmosphere. The procedure for calculating such fluxes is described below, whereas their sensitivity to 3DNEPH, SFCOBS, and zonal mean 3DNEPH monthly mean analyses of layered cloud amount is discussed in section 5. The present calculations are limited to two specific months, i.e., January 1977 and July 1979, although the climatological mean sensitivity is of ultimate interest. The term "model-diagnosed" signifies that the radiative fluxes are calculated by a cloud-radiation model from "observed" atmospheric data, i.e., monthly mean analyses of temperature T and water vapor mixing ratio r.

The temperature analyses for January 1977 and July 1979 were derived from 12-hourly analyses generated by the National Meteorological Center (NMC). Some sample vertical profiles of observed zonal mean temperature at one tropical
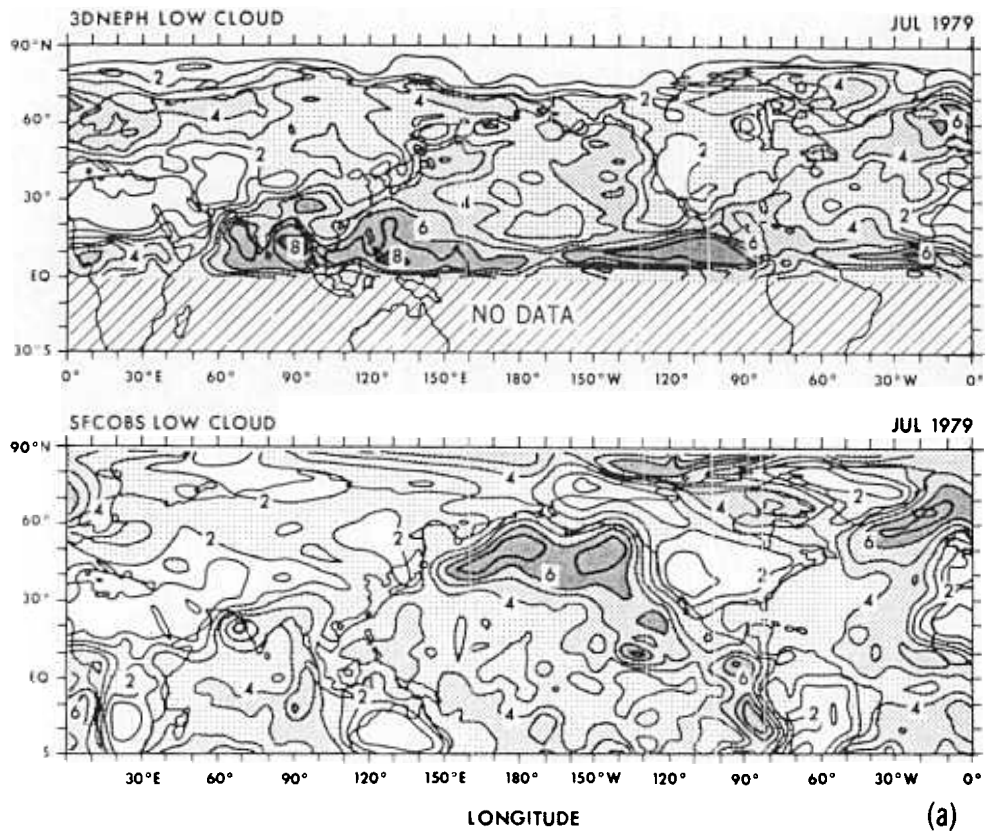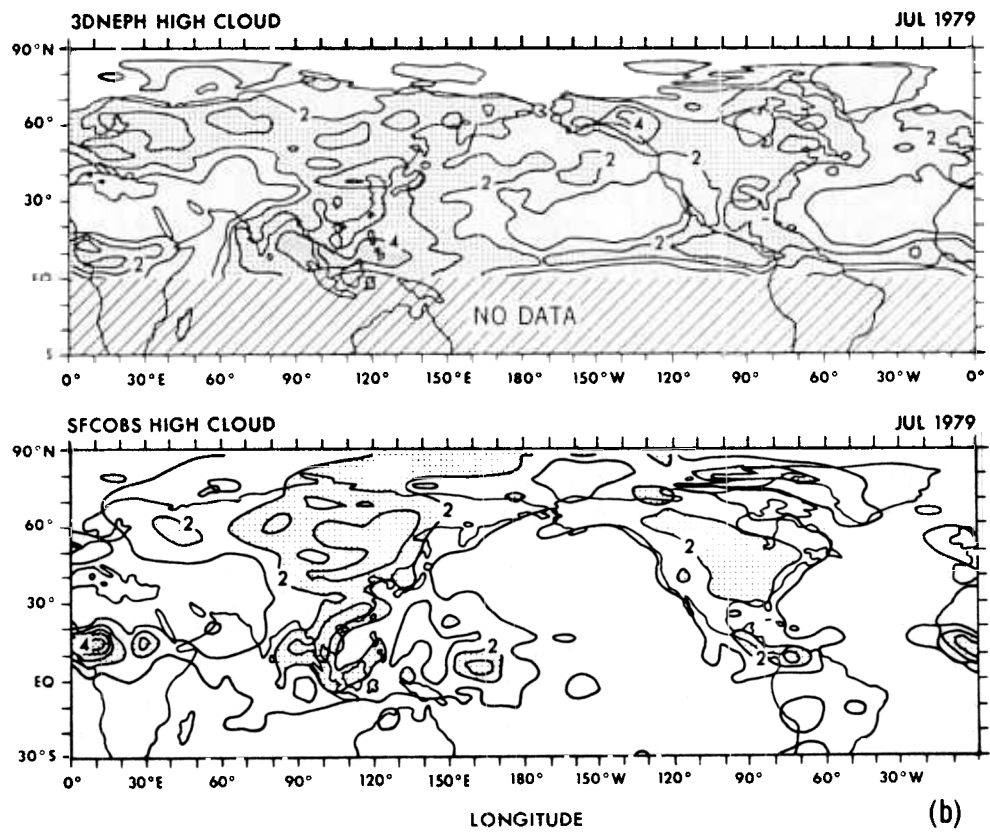
Fig 5a

(a)

Fig 5b

(b)

3DNEPH TOTAL CLOUD   JUL 1979

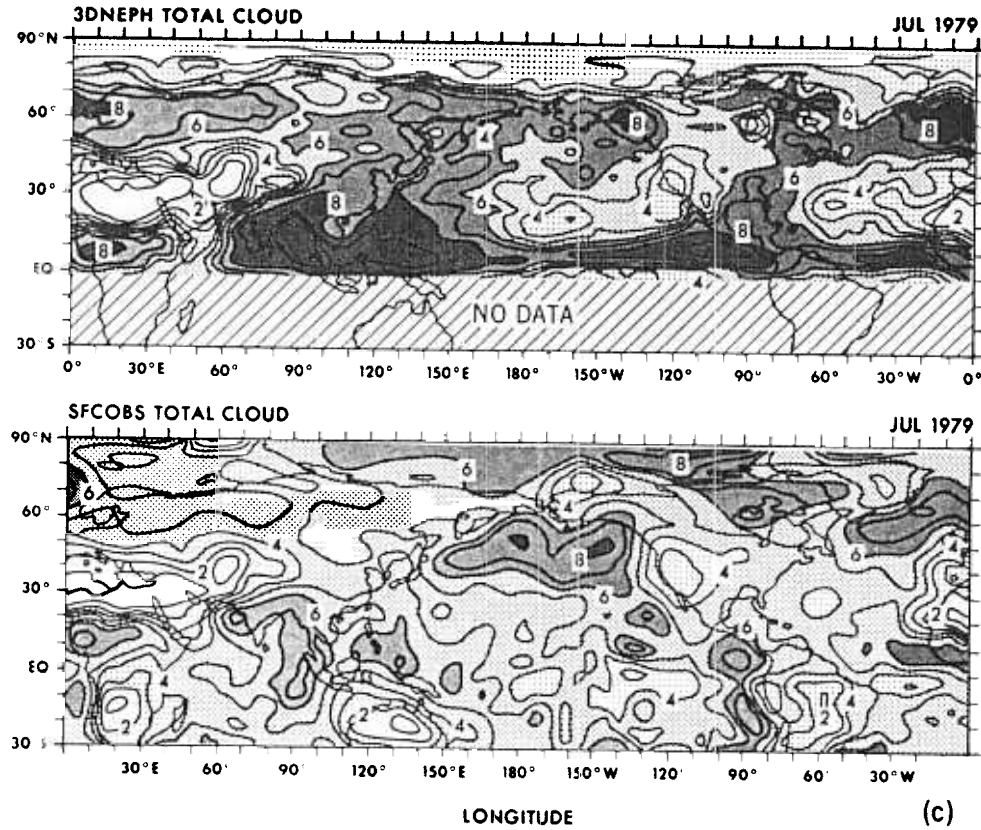SFCOBS TOTAL CLOUD   JUL 1979

LONGITUDE   (c)

Fig 5c

Fig. 5.   Same as Fig. 4, except for July 1979.

and one extratropical latitude are illustrated for January 1977 and July 1979 in Figure 9. Meanwhile, according to *Rosen and Salstein* [1980], the NMC analyses of r during January 1977 were very biased in the middle troposphere. Therefore, an optimum interpolation (OI) analysis of temperature and dewpoint station data was performed to obtain r. The OI scheme is similar to the one employed by *Ploshay et al.* [1983], except that climatological first guess fields were used. The January 1977 monthly mean analysis of mixing ratio at 850 mbar, i.e., r_{850} is depicted in Figure 10.

The cloud-radiation model is part of a complicated GFDL global spectral GCM. In practice it was more convenient to work with the full model rather than to decouple the cloud radiation model. Normally, the full model is integrated in time. In this instance, though, the calculations were terminated as soon as the initial tendencies were evaluated. By that time the model-diagnosed radiative fluxes at the top and bottom of the atmosphere and the radiative heating rates in its interior had been calculated and archived. The same procedure was repeated for each specification of cloud amount. The monthly means of the daily NMC temperature and wind analyses and the monthly mean OI water vapor analysis served as "initial conditions."

The GFDL global spectral model itself has been described in detail by *Gordon and Stern* [1982]. It has physical processes commonly associated with GCM's. Some relevant nonradiative aspects of the model are briefly summarized below. The moderate resolution R21L09 "E4" version is employed, where R21 denotes rhomboidal truncation at zonal wave number 21; L09 denotes the nine unequally spaced sigma levels, i.e., 0.009, 0.074, 0.189, 0.336, 0.500, 0.665, 0.811, 0.926, and 0.991; and the vertical coordinate, sigma, is the ratio of pressure to sur-

face pressure. The radiative fluxes are evaluated on the model's tranform grid containing 54 latitudes and 64 longitudes. "E4" denotes the parameterization of vertical turbulent mixing. Its distinctive features are a static stability-dependent Monin-Obukhov formulation in the surface boundary layer; a Richardson, number-dependent, Mellor-Yamada [*Mellor and Yamada*, 1974] turbulent closure scheme in the planetary boundary layer and free atmosphere; and suppression of dry convective adjustment. Over the open ocean, a monthly mean climatology is prescribed for the surface tem-
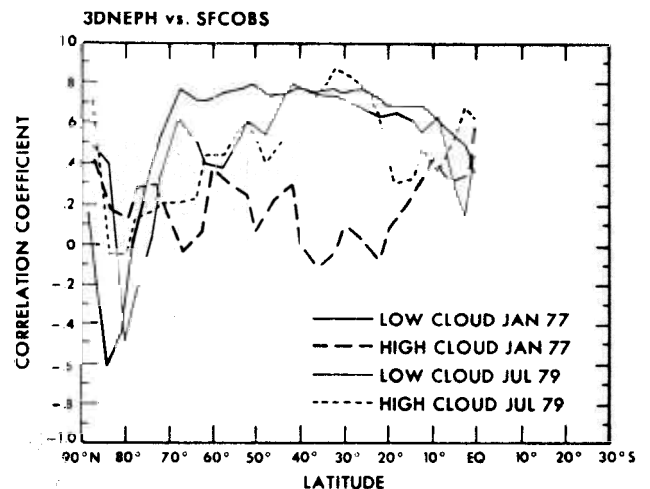

3DNEPH vs. SFCOBS

Fig. 6.   Longitudinal correlation between the 3DNEPH and SFCOBS analyses of low and high cloud amount vs. latitude for January 1977 and July 1979. The domain is 90°N to 0°.
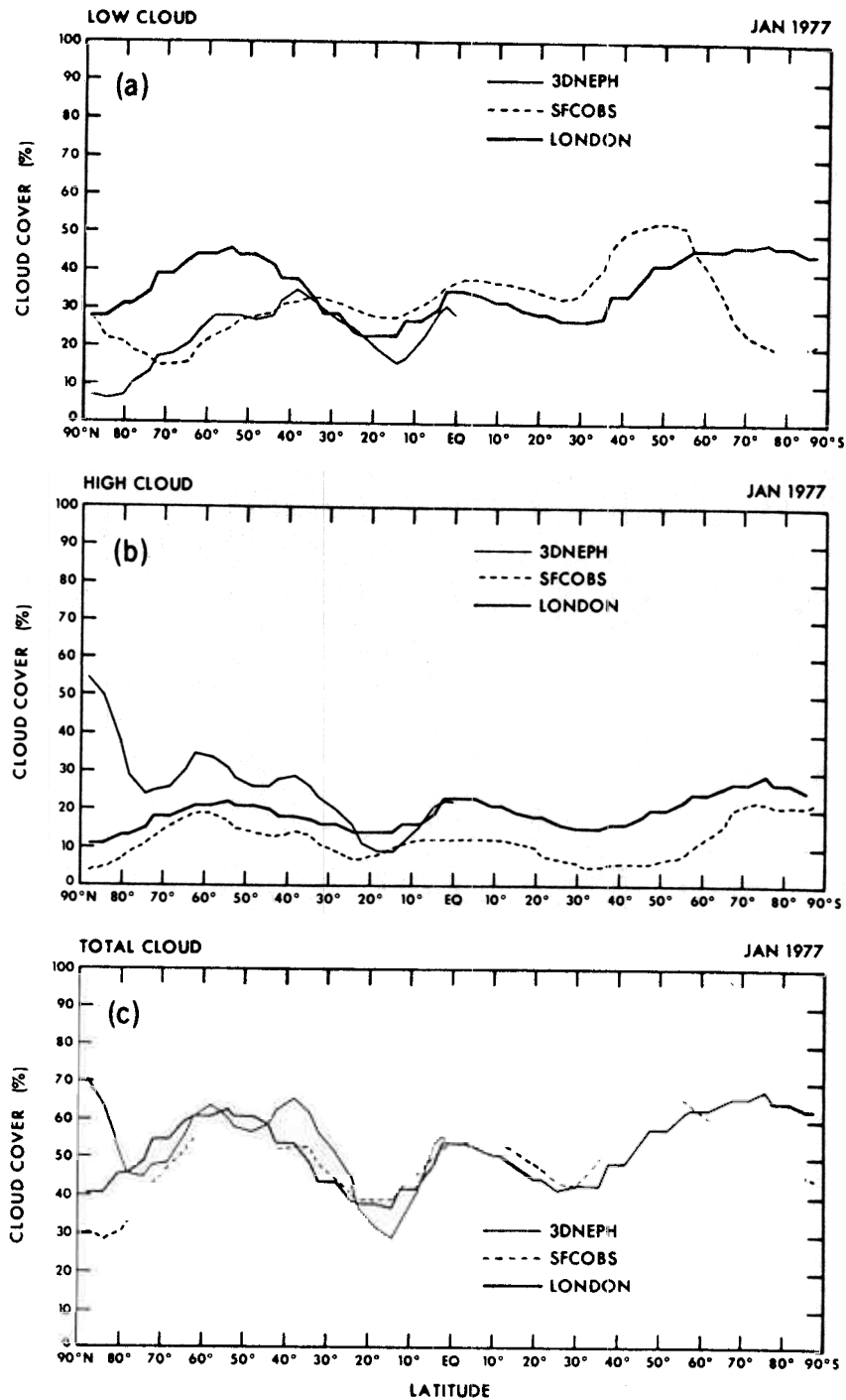
Fig. 7. Latitudinal profiles of different analyses of zonal mean cloud amount for January 1977: (a) low clouds, (b) high clouds, (c) total clouds. The domain is 90°N–90°S.

perature T_s. But over land and sea ice, T_s is obtained by solving a diagnostic surface heat balance equation. The T_s field for January 1977 (given 3DNEPH clouds) is illustrated in Figure 11.

In the context of the present study the cloud-radiation model is a very essential component of the spectral GCM. The relatively accurate radiation algorithms and efficient radiation code of Fels and Schwarzkopf [1975] is employed. Its efficiency is attributed to the Fels-Schwarzkopf hereafter referred to as FS, simplified exchange method of calculating infrared cooling caused by water vapor and an optimized computer code. The

FS longwave code utilizes accurate CO_2 transmission functions [see Fels and Schwarzkopf, 1981] and has a Bignell [1970] water vapor continuum. Absorption within the continuum region varies approximately as the square of the water vapor concentration. The FS shortwave code uses the Lacis and Hansen [1974] parameterization of absorption by ozone and water vapor and incorporates multiple reflection.

The daily mean solar zenith angle is a function of latitude and time of year, i.e., diurnal variation is suppressed. The solar constant is ~ 1368 W m^{-2} (1.96 Ly min^{-1}).

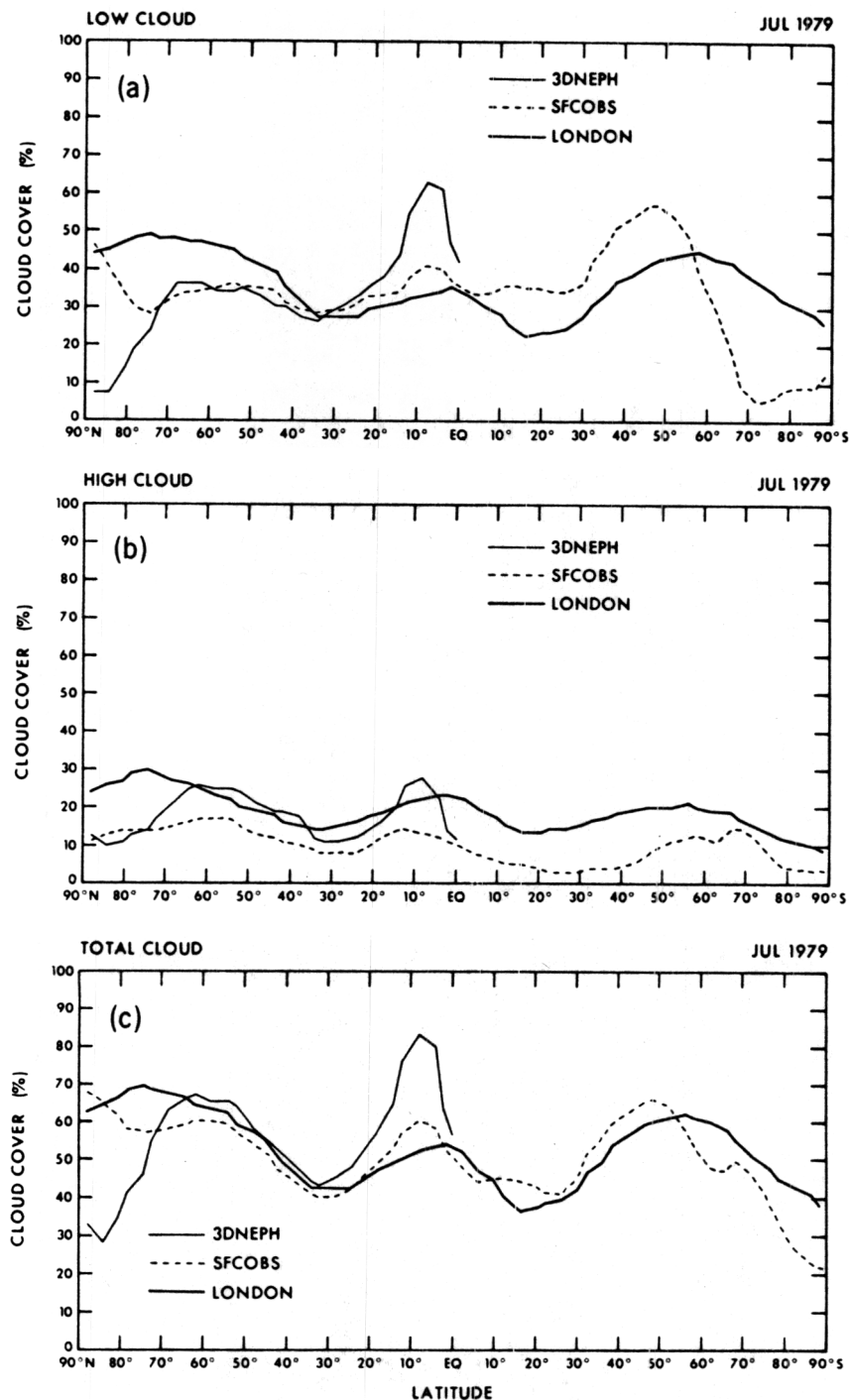Another aspect of the cloud-radiation model is the specifi-

Fig. 8.   Same as Fig. 7, except for July 1979.

cation of the radiatively active constituents, i.e., ozone, carbon dioxide, water vapor, and clouds. The concentration of ozone is seasonally varying as well as latitude and height dependent. This climatology is based upon data compiled by *Hering and Borden* [1965] and *London* [1962]. An annual mean climatology is specified for CO_2, corresponding to a constant mixing ratio of 330 ppm. As previously mentioned, observed January 1977 or July 1979 monthly mean OI analyses of water vapor mixing ratio r are employed.

The cloud-radiation model makes provision for three layers of randomly overlapped clouds. In nature a single thick convective cloud could exist rather than three distinct layers. But the specified cloud analyses, i.e., 3DNEPH, SFCOBS, or zonal mean 3DNEPH, do not explicitly discriminate between convective vs. stratiform clouds. The fixed heights of the cloud tops and bases were adapted from the *Telegadas and London* [1954] winter or summer climatologies. They are illustrated schematically in Figure 1 as a function of latitude. The albedos and absorptivities of low, middle, and high clouds were adapted from *London* [1957] and correspond to the standard values of Table 1, unless otherwise noted. The optional values, which take into account measurements reported by *Drummond and Hickey* [1971], *Wiscombe* [1975], and *Cess* [1976], are used in section 6. The emissivities of low, middle, and high

TABLE 2. Mean Fractional Cloud Amount

Case	Layer	Mean	3DNEPH	SFCOBS	LONDON
January 1977	High	GBL		0.109	0.187
		NH	0.218	0.119	0.174
		SH		0.099	0.199
	Middle	GBL		0.119	0.084
		NH	0.196	0.119	0.084
		SH		0.120	0.083
	Low	GBL		0.338	0.339
		NH	0.249	0.286	0.329
		SH		0.389	0.350
	Total	GBL		0.489	0.504
		NH	0.503	0.455	0.488
		SH		0.522	0.520
July 1979	High	GBL		0.094	0.183
		NH	0.187	0.121	0.198
		SH		0.067	0.169
	Middle	GBL		0.116	0.083
		NH	0.251	0.127	0.083
		SH		0.105	0.082
	Low	GBL		0.357	0.339
		NH	0.376	0.338	0.352
		SH		0.375	0.326
	Total	GBL		0.491	0.501
		NH	0.587	0.493	0.520
		SH		0.490	0.483

clouds are all assumed to be unity, except in one case in section 6. As for surface albedo A_s the zenith-angle-dependent formulation of *Payne* [1972] is used over the open oceans. Also, $A_s = 0.75$ over the permanent snow pack, i.e., poleward of 70°, and

$$A_s = [\min(A_{s_0} + (0.60 - A_{s_0})(d/10)^{1/2}, 0.60] \quad (2)$$

over land and sea ice equatorward of 70°, where A_{s_0} is the surface albedo in the absence of snow cover and d is the snow depth in centimeters. A_{s_0} is assigned the value 0.50 over sea ice and is based upon the analysis of *Posey and Clapp* [1964] over land. In the northern hemisphere, d was reconstructed, unless otherwise stated, from an AFGWC map analysis of "observed" weekly mean snow depth for the first week of January 1977. The AFGWC analysis scheme utilizes surface observations, where available, but permits d to relax gradually toward climatology in data void regions. However, zero snow cover is assumed unless the observed, satellite-dependent brightness exceeds a threshold value. In the southern hemisphere a GFDL GCM climatological snow depth field was specified. The resulting surface albedo field A_s is illustrated in Figure 12a. For comparative purposes the surface albedo field corresponding to GCM climatological snow cover in both hemispheres is shown in Figure 12b. The large discrepancy over North America and Asia between Figures 12a and 12b is due entirely to differences between the observed AFGWC vs. GCM climatological snow cover. The AFGWC snow cover is certainly more realistic than GCM climatology over North America.

The model-diagnosed radiative fluxes are influenced by cloud amount, specification of the various other cloud parameters, observed temperature and water vapor fields, surface temperature, and surface albedo. Moreover, application of moist convective adjustment may slightly alter the observed vertical temperature and water vapor profiles and hence the longwave radiative flux. The "E4" physics and prescribed ob-

served vertical temperature profile in the boundary layer, as well as clouds, can also affect T_s over land and sea ice.

5. SENSITIVITY OF RADIATIVE FLUXES TO CLOUD AMOUNT

Model-diagnosed monthly mean radiative fluxes were calculated for January 1977 and July 1979, using the approach outlined in section 4. Their sensitivity to the specification of cloud amount was evaluated by holding all input parameters, except cloud amount, fixed. Comparative results are presented for zonal mean 3DNEPH and geographically varying 3DNEPH and SFCOBS cloud analyses. The emphasis is upon radiative fluxes at the top of the atmosphere, for which satellite verification data is available. In principle the 3DNEPH cloud analysis could be more suitable for radiation calculations than the SFCOBS, since it is based mainly on satellite data.

First, fields of model-diagnosed longwave radiative flux F and reflected shortwave flux $S\uparrow$, are compared with satellite-derived observations. The region poleward of 30°S has been omitted in the SFCOBS analyses because of the lack of SFCOBS cloud data, and the 3DNEPH analysis terminates at the equator. "WINSTON OBS" and "ZM" denote the satellite verification data and zonal mean, respectively. The "WINSTON OBS" monthly mean radiative fluxes were calculated from daily earth radiation budget (ERB) fields archived by the National Environmental Satellite Data Information Service (NESDIS) on a 2.5° × 2.5° latitude-longitude grid [*Gruber*, 1978]. The ERB archives for January 1977 and July 1979 were derived from scanning radiometer measurements by the NOAA 5 and TIROS-N satellites, respectively. The monthly mean fluxes were linearly interpolated to the coarser GCM grid. A correction factor had to be applied to the observed
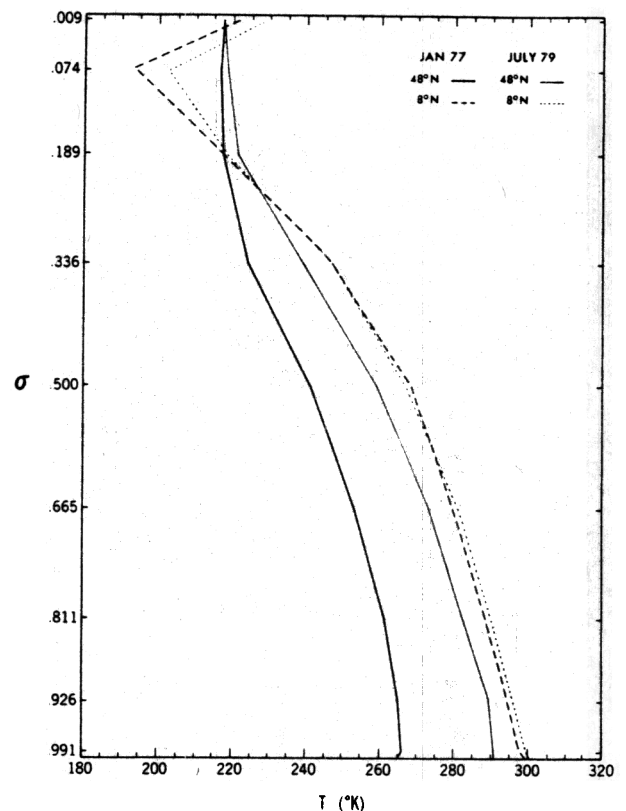

Fig. 9. Vertical profiles of observed, monthly mean–zonal mean temperature at 48°N and 8°N for January 1977 and July 1979.

r_{850} (g/kg)   JAN 1977
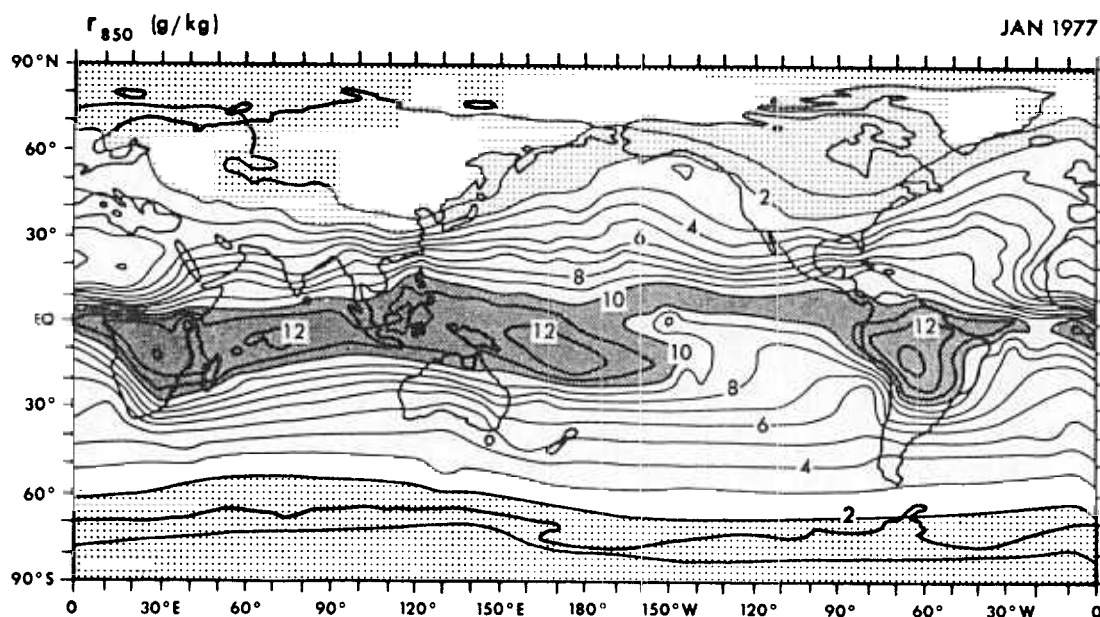
Fig. 10. Monthly mean optimum interpolation analysis of water vapor mixing ratio at 850 mbar for January 1977 over the 90°N–90°S domain. Contour interval = 1 g/kg.

longwave fluxes, as discussed in Appendix B, because of a bias in the NESDIS data.

The model-diagnosed outgoing longwave flux F (Figures 13a and 14a) is very sensitive to the specification of cloud amount in the tropics and in the summer hemisphere extratropics. With zonal mean 3DNEPH clouds, F is nearly zonally symmetric. With SFCOBS clouds, F exhibits some longitudinal variation, although less than observed. Note that the SFCOBS minima are too weak over oceanic segments of the ITCZ, where surface-based cloud observations are sparse. In contrast, the 3DNEPH tropical outgoing longwave flux corresponds more closely to observation.

In the northern hemisphere winter extratropics the longitudinal variation of F is controlled predominantly by surface temperature T_s (cf. Figures 11 and 13a, and see Figure 17). Two factors are involved: Most importantly, the land-sea con-

trast in T_s is very large; second, there is less temperature contrast between low cloud top level and the earth's surface at mid-latitudes in winter than in summer or in the tropics (cf. Figures 1 and 9). Nonetheless, F is somewhat sensitive to cloudiness in the winter extratropics, with the 3DNEPH flux verifying better, for the most part, than SFCOBS. Incidentally, the outgoing longwave flux is very insensitive to zonal mean vs. geographically varying water vapor (not shown) in the tropics and extratropics.

Like F, the reflected shortwave flux $S\uparrow$ is more zonally asymmetric in the tropics (Figures 13b and 14b) for longitudinally varying (as compared to zonal mean) 3DNEPH cloud amounts. But the correspondence between 3DNEPH model diagnosis and observation is poorer for $S\uparrow$ than for F in the tropics as well as the extratropics. Meanwhile, during January 1977, $S\uparrow$ is qualitatively simulated over southern Africa and

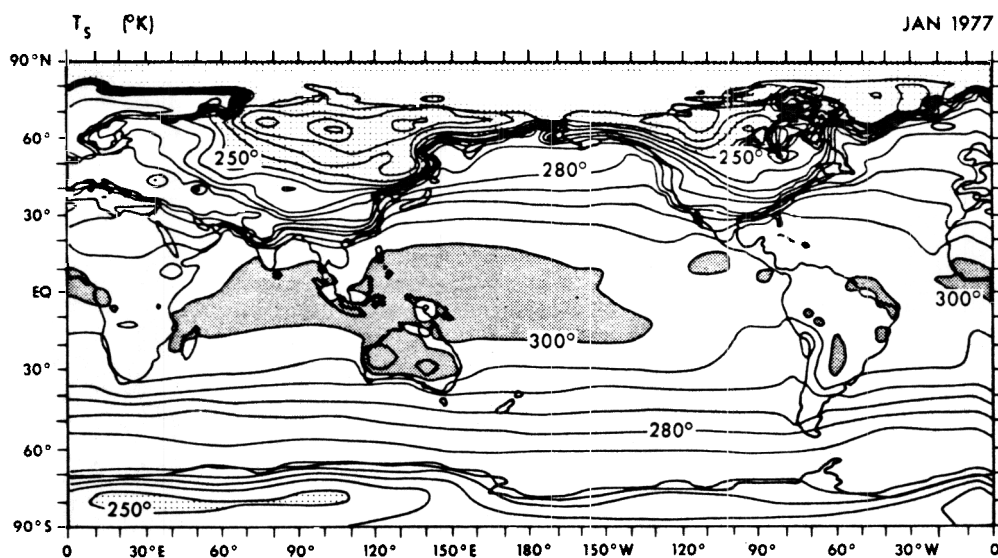T_s (°K)   JAN 1977

Fig. 11. Monthly mean surface temperature field for January 1977 as specified over open water and model diagnosed over land and sea ice. Domain is 90°N–90°S, contour interval is 5 K.
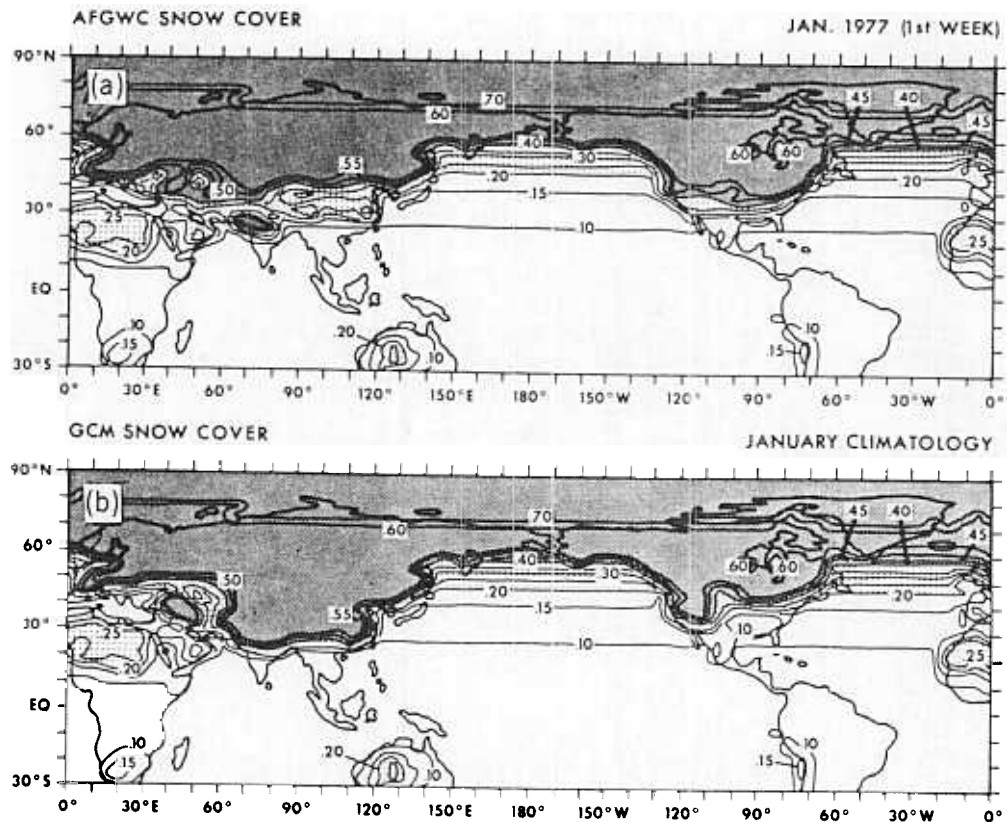
Fig. 12. The January 1977 surface albedo field within the 90°N–30°S domain, assuming (a) standard snow cover, i.e., AFGWC (NH)/GCM climatology (SH) and (b) GCM climatology in both hemispheres. Contour interval = 0.05 or 0.10.

Brazil in the SFCOBS panel, even though SFCOBS clouds utilize no satellite data. This result is consistent with the SFCOBS analysis of low cloud amount (see Figure 4a) and the greater reflectivity of low (vs. high) clouds (Table 1).

The model-diagnosed, monthly mean short- and/or long-wave radiative fluxes are susceptible to several sources of error. For example: (1) the specification of cloud albedos, emissivities, tops, and bases is relatively crude; (2) the specification of surface albedo may be inaccurate, especially over snow-covered land; (3) nonlinear transient effects are not fully represented, since the fluxes are evaluated from monthly mean, rather than daily temperature, mixing ratios and cloud amount fields; (4) aliasing errors arise because of the once or twice per day synoptic sampling of radiances from sun-synchronous polar-orbiting satellites; (5) the NOAA 5 (or TIROS-N) satellite, DMSP satellite, and surface observations within a particular grid square are taken at different times of the day. Regarding this latter point, during July 1979, the TIROS-N satellite measured shortwave flux at approximately 1530 hours local time, when convection is near its maximum intensity in many regions. In contrast the AFGWC 3D-Neph analysis utilized DMSP satellite data measured in the early morning or early evening, as well as near midday, whereas surface-based observations were reported up to several times per day or not at all.

The net radiative flux R (where $R = S - F$) is a more important parameter for climate than F or S. Thus, although longitudinally varying cloudiness appears to be moderately beneficial to F or S outside of the winter extratropics, the verification of R provides a more crucial test. This test is quite stringent in the tropics, where R tends to be residual of S and F.

In January 1977 the longitudinal structure of R (not shown) is masked by the meridional gradient of incoming solar radiation north of 25°N or 30°N. Moreover, the role of clouds is masked by the influence of A_s and, especially, T_s in the extratropics. In July 1979 (Figure 14c), R is indeed sensitive to zonal mean vs. longitudinally varying cloudiness. But unfortunately, the model-diagnosed net radiative flux field corresponds rather poorly with WINSTON OBS over the North Atlantic, North Pacific, and subtropical Pacific oceans and elsewhere, irrespective of whether longitudinally varying or zonal mean cloudiness is specified.

As supplementary verification we cross-correlated model-diagnosed vs. WINSTON OBS eddy radiative fluxes at each latitude. For example the correlation coefficient for F is defined as

$$r_F = \frac{\langle F_m' F_o' \rangle}{\langle F_m'^2 \rangle^{1/2} \langle F_o'^2 \rangle^{1/2}} \qquad (3)$$

As in equation (1), angle brackets denote zonal means and primes denote eddies, i.e., departures from zonal means. Also, m and o represent the model-diagnosed and WINSTON OBS fluxes, respectively. Correlation coefficients for F, $S\uparrow$ and R are defined in analogous fashion. Latitudinal profiles of correlation coefficients r_F (Figure 15a) and $r_{S\uparrow}$ (Figure 15b) are shown for winter only, and r_R for winter (Figure 15c) as well as summer (Figure 16). Note that $r_{S\uparrow} = r_S$, since the incoming solar flux is zonally symmetric.

The tendency for r_F to exceed $r_{S\uparrow}$ during January 1977 is consistent with the subjective map verification. Within the 30°N–5°N low-latitude belt, the 3DNEPH model-diagnosed fluxes verify best with $r_F \sim 0.8$ and $r_{S\uparrow} \sim 0.6$ to 0.7. In con-

trast, if zonal mean 3DNEPH clouds are specified, the model-diagnosed F is poorly correlated and $S\uparrow$ essentially uncorrelated with WINSTON OBS in the tropics.

The results for r_R are less impressive than for r_F or r_S, especially in the tropics. In January 1977 (Figure 15c) a meaningful, positive r_R correlation is not found within the 15°N–0°N latitude belt for any of the three cloud distributions. Between 15°N and 25°N, positive correlations of comparable magnitude are obtained for asymmetric as well as zonal mean 3DNEPH clouds, whereas r_R is negative for SFCOBS clouds. The behavior near 25°N may be affected by land surface albedo, and the relatively high correlations in the winter extratropics are probably associated with the longitudinally varying surface temperature field.

In July 1979 (Figure 16) the r_R correlations remain poor in the 15°N–0° latitude belt, which contains the ITCZ. The relatively better performance of the asymmetric and zonal mean 3DNEPH clouds (as compared to SFCOBS) poleward of 15°N now extends to approximately 40°N. However, within the 45°N–60°N summer cyclone belt, the correlation is actually negative for 3DNEPH and zonal mean 3DNEPH clouds and only weakly positive for SFCOBS clouds.

Latitudinal profiles of the correlation between observed eddy radiative flux and selected meteorological variables, including 3DNEPH cloud amount, illustrate the relative importance of such variables for the observed radiation budget of January 1977. For example, analogous to equation (3),

$$r_{FT_s} = \frac{\langle F_0' T_s' \rangle}{\langle F_0'^2 \rangle^{1/2} \langle T_s'^2 \rangle^{1/2}} \tag{4}$$

and

$$r_{Fn_h} = \frac{\langle F_0' n_h' \rangle}{\langle F_0'^2 \rangle^{1/2} \langle n_h'^2 \rangle^{1/2}} \tag{5}$$

where r_{FT_s} is the longwave flux–surface temperature correlation, r_{Fn_h} is the longwave flux–3DNEPH high cloud amount correlation, F_0 is the WINSTON OBS longwave flux, and T_s is the surface temperature. For outgoing longwave flux (Figure 17) the controlling influences of high cloudiness in the tropics and of surface temperature T_s in the winter extratropics are confirmed. Also, F is negatively correlated with T_s in the tropics, since deep convection tends to be positively correlated with T_s. In the northern hemisphere winter extratropics, F is positively correlated with water vapor mixing ratio at 850 mbar and with low cloud amount but uncorrelated with high cloud amount. There, specified low cloud tops are nearly as warm as the surface, and r_{850} and n_l are probably positively correlated with T_s.

Figure 18 reveals that the observed, reflected shortwave flux is primarily controlled by the surface albedo A_s in the northern hemisphere winter extratropics and by high cloudiness in the tropics. At high northern latitudes, e.g., 60°N–70°N, the lack of any strongly positive correlations is probably due to enhanced relative error in $S\uparrow$ and/or an imperfect specification of A_s over sea ice and permanent snow cover. Within the 40°N–55°N latitude zone, $S\uparrow$ is more highly correlated with n_h and A_s than with n_l. This latter result is consistent with the longitudinal distributions of snow cover (hence A_s), n_l, and n_h, and their relative contributions to $S\uparrow$ over land and over sea.

In the tropics and subtropics (excluding deserts and snow-covered terrain), clouds should play a more important role than A_s. Cloud analyses based primarily upon longwave flux

data may seriously underestimate low stratus and/or may categorize thick convective clouds as high (thin) clouds. This may explain why $S\uparrow$ is more highly correlated with n_h than with n_l in the northern hemisphere tropics.

Differential zonal mean longwave (ΔF), shortwave (ΔS), and net (ΔR) radiative fluxes (where $\Delta R = \Delta S - \Delta F$) have been calculated by subtracting the relevant WINSTON OBS flux from the corresponding model-diagnosed flux. Departures of ΔF, ΔS, or ΔR from zero may be interpreted as biases in the model-diagnosed fluxes. Strictly speaking, a negative adjustment of 1 or 2 W m^{-2} in the extratropics and 2 to 5 W m^{-2} in the tropics should be applied to ΔS and ΔR. The necessity of this calibration stems from a discrepancy between the value of the solar constant S_0 assumed by NESDIS (~ 1353 W m^{-2}) and that assumed in our cloud-radiation model (~ 1368 W m^{-2}).

The uncalibrated latitudinal profiles of ΔF, ΔS, and ΔR for January 1977 are illustrated in Figures 19a, b, and c, respectively. The SFCOBS and LONDON zonal mean longwave fluxes possess a substantial positive bias in the northern hemisphere extratropics, as do all of the model-diagnosed longwave fluxes near the equator. Conversely, model-diagnosed shortwave and net fluxes possess negative bias in the tropics, where the dominant ΔS contribution is reinforced by the ΔF contribution. Overall, the 3DNEPH zonal mean net radiative flux verifies somewhat better than SFCOBS or LONDON.

In July 1979 (not shown) the 3DNEPH ΔF bias is quite weak throughout the northern hemisphere, whereas the SFCOBS ΔF exceeds $+25$ W m^{-2} in the ITCZ. The 3DNEPH and SFCOBS ΔS curves both attain maximum values of $\sim +15$ W m^{-2} near latitude 50°N. In the ITCZ (~ 8°N) the 3NDEPH ΔS approaches -40 W m^{-2} at 8°N, tapering off to -20 W m^{-2} on either side. Meanwhile, the 3DNEPH ΔR peaks ($\sim +15$ W m^{-2} at 50°N and -35 W m^{-2} at 8°N) are slightly sharper than the corresponding SFCOBS peaks. The ΔR bias for LONDON climatological clouds is much smaller. However, this result is due to a fortuitous cancellation between ΔS and ΔF. In contrast the bias in 3DNEPH ΔS is essentially unbalanced.

The above results are consistent with the relatively greater amount of 3DNEPH (as compared to SFCOBS or LONDON) high clouds in the January 1977 extratropics and the greater amount of 3NDEPH low and high clouds in the July 1979 ITCZ. The AFGWC 3D-Neph analysis procedures [see Fye, 1978] may tend to overestimate the low cloud amount in the latter region. The fact that the cloud albedos were actually reduced for the July 1979 case (see Table 1) lends some credence to this hypothesis. Also, other cloud-related parameters could contribute to biases, as explored in section 6.

Incidentally, the ΔF's (or ΔS's) corresponding to 3DNEPH and zonal mean 3DNEPH clouds nearly coincide in January 1977 and deviate from each other by less than 5 W m^{-2} in July 1979. In other words, zonally asymmetric cloudiness primarily affects the longitudinal variation of the radiative flux rather than its zonal mean value.

We have focused on radiative fluxes at the top of the atmosphere, where satellite verification data is readily available. Next, we briefly discuss the sensitivity of the net (downward) radiative flux at the earth's surface to 3DNEPH vs. zonal mean 3DNEPH cloud amount. The motivation is that cloud amount could modulate the heating of the oceanic mixed layer, especially in summer, thereby indirectly affecting the seasonal forcing of the atmosphere. Global surface verification
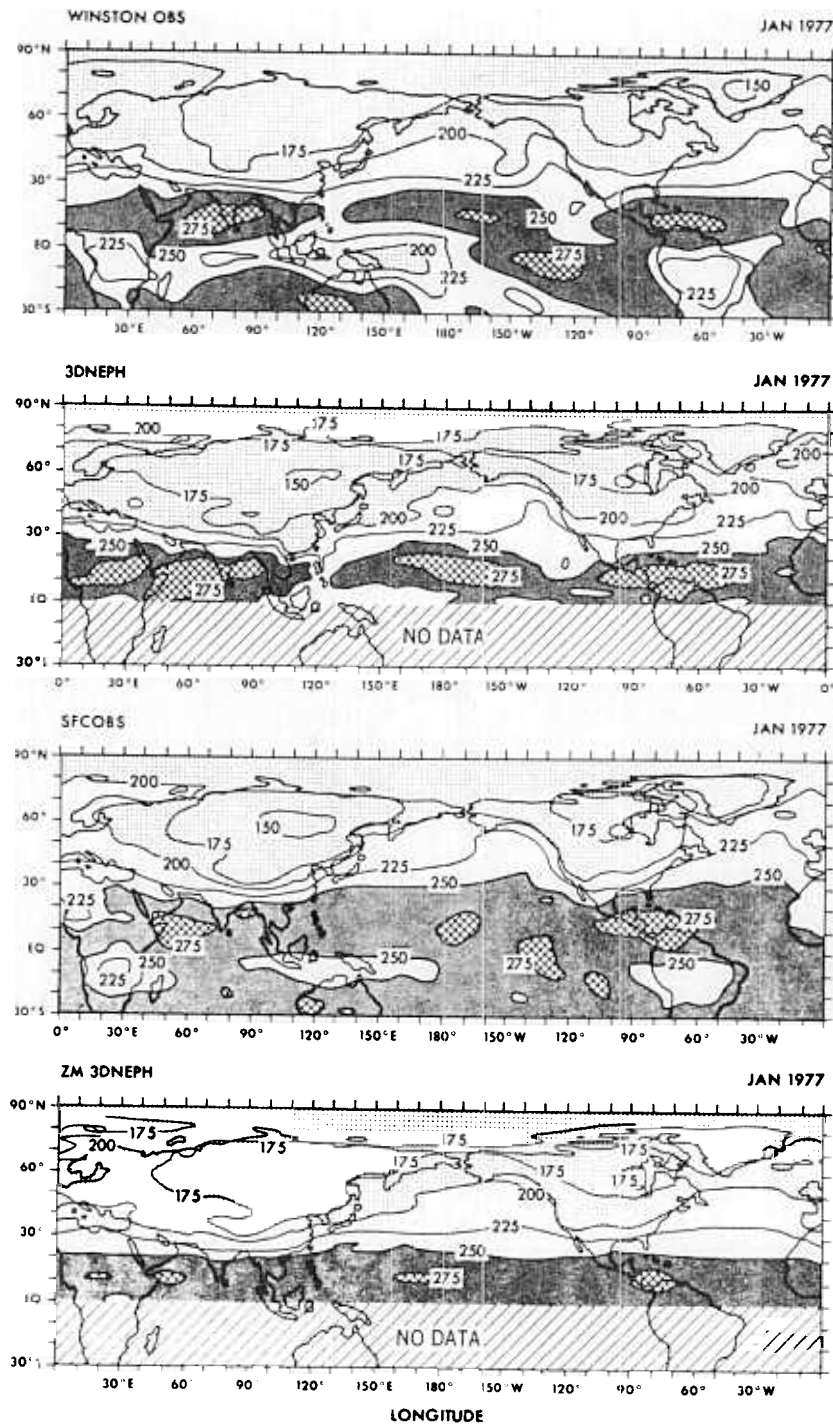
Fig 13a

data for the net flux is essentially nonexistent (although insolation data is available, mostly over North America). The model-diagnosed results for July 1979 are illustrated in Figure 20. Note that the specification of longitudinally varying 3DNEPH cloudiness tends to diminish the model-diagnosed net flux over the western tropical and subtropical Pacific and Atlantic oceans by as much as 25 W m^{-2} and to enhance it further east by a similar amount. Thus the net flux at the surface tends to decrease where the 3DNEPH low cloudiness exceeds its zonal mean value, and the converse is also true. In other words the reflectivity effect of the clouds tends to outweigh their greenhouse effect in the above regions.

The sensitivity of the model-calculated surface temperature T_s to longitudinally varying vs. zonal mean (3DNEPH) cloudiness was monitored over land. During July 1979, the response was negligible. During January 1977 (Figure 21), the longitudinally varying 3DNEPH clouds appeared to modulate the longwave cooling, i.e., T_s tended to increase over western Europe and decrease over Siberia and Canada. The magnitude of the effect was only of $O(2$ K$)$, perhaps because variations in zonal mean cloudiness were typically ≤ 0.2 over the extratropical continents. *Stephens and Webster* [1981] obtained a greater response, but they compared idealized extreme conditions, i.e., overcast vs. clear conditions. Second, extremes in
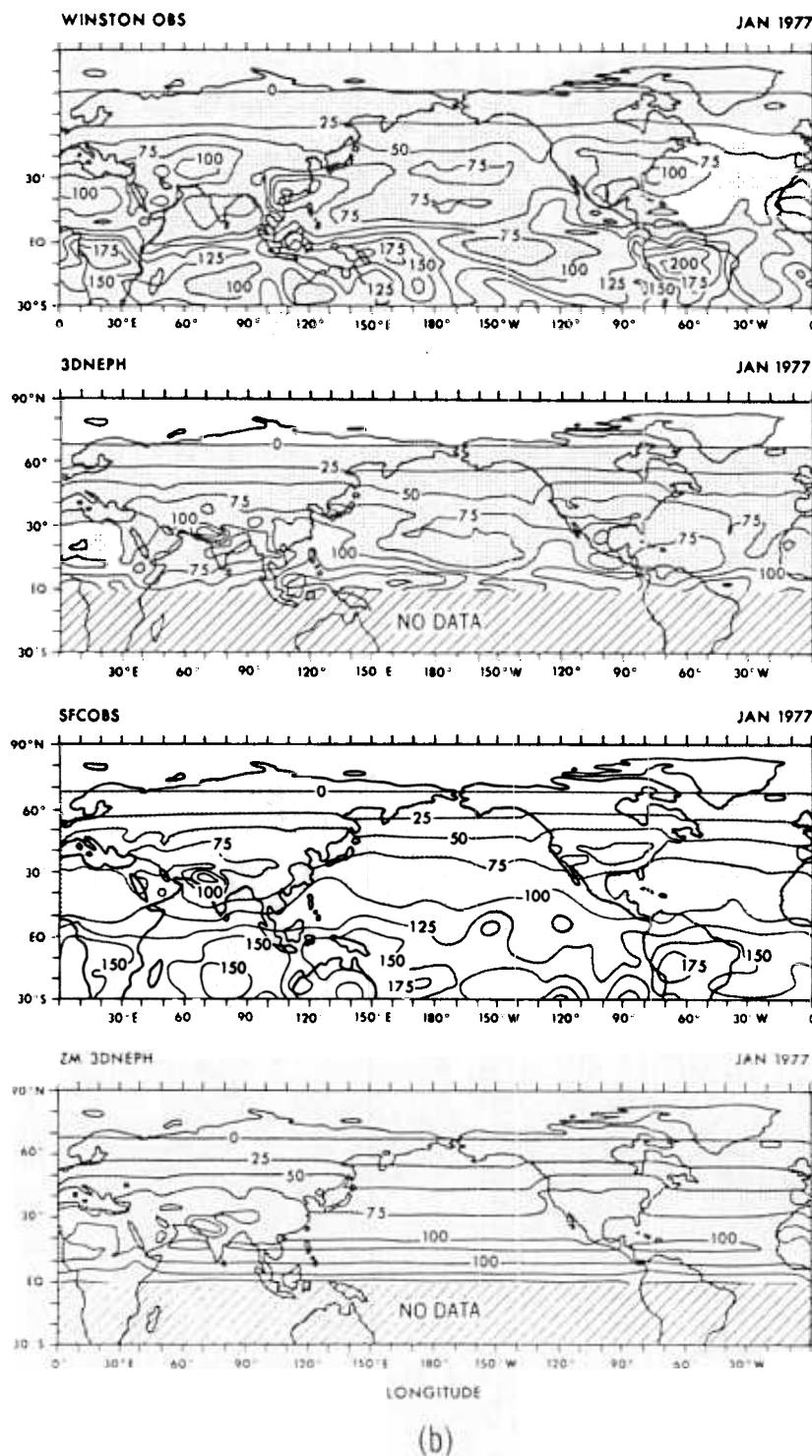
Fig. 13. Observed and model-diagnosed radiative flux fields for January 1977: (a) outgoing longwave and (b) reflected shortwave flux. The domain is 90 N-30 S. Contour interval = 25 W m^{-2}.

longwave cooling and insolation were tempered by ignoring the diurnal variation of the temperature field and incoming solar radiation.

6. SENSITIVITY OF RADIATIVE FLUXES TO OTHER CLOUD PARAMETERS AND SNOW COVER

Knowledge of the sensitivity of radiative fluxes to cloud parameters other than cloud amount and to snow cover

would help place the sensitivity results of section 5 in better perspective. For example, is "cloud amount" a relatively important parameter, as we have tacitly assumed? Moreover, it may be useful to check whether the use of more accurate values of radiative parameters in our cloud-radiation model yields improved model-diagnosed radiative fluxes. For these reasons we have briefly investigated the sensitivity of our model-diagnosed radiative fluxes to the longwave emissivity ε_{LW} of high clouds, the vertical placement of high clouds,
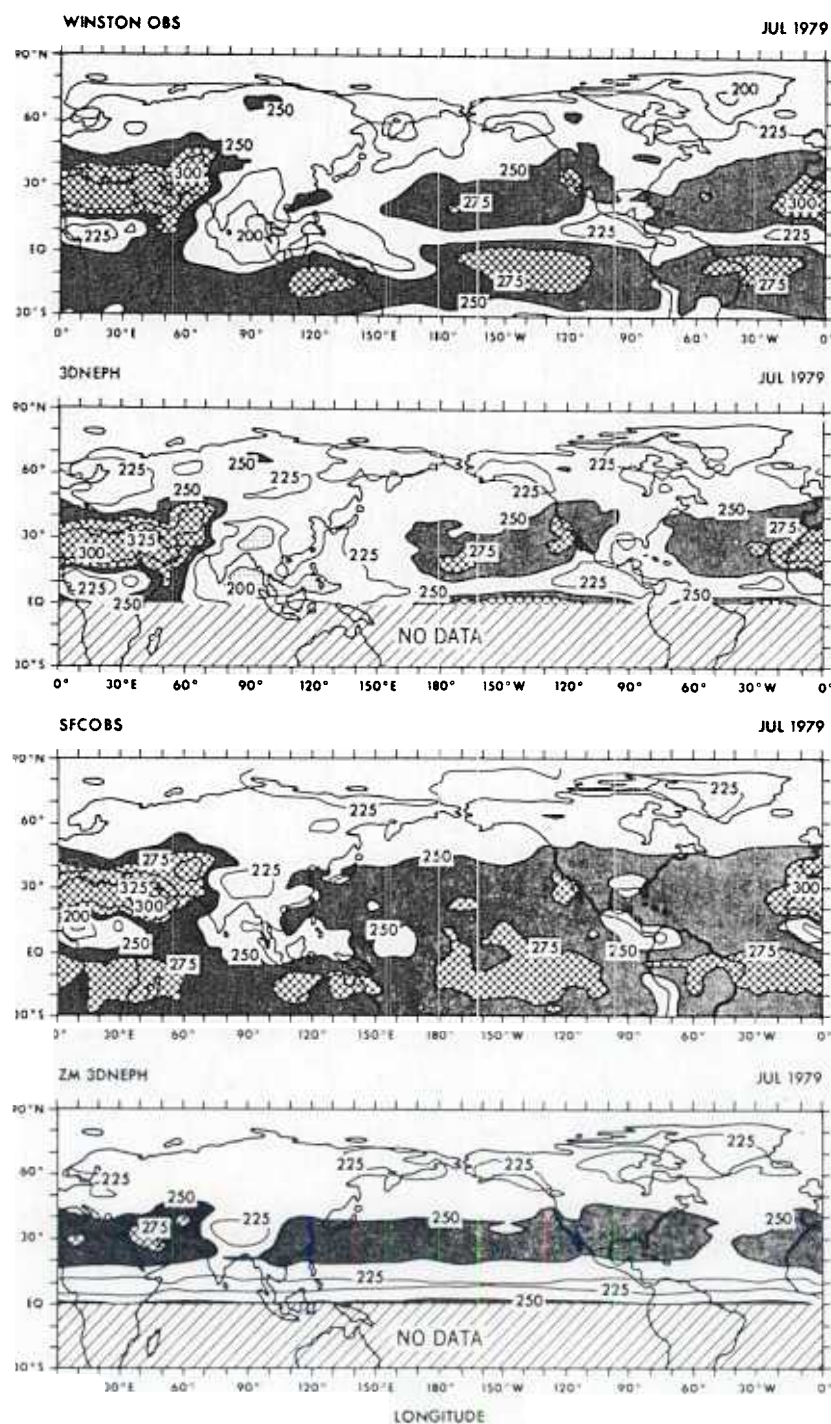
Fig. 14a

cloud albedo, and snow cover. The above parameters were individually varied while the January 1977 3DNEPH cloud amount fields and monthly mean meteorological analyses were held fixed.

The January 1977 results for the zonal mean differential outgoing longwave flux ΔF and differential absorbed short-wave flux ΔS are depicted in Figures 22a and 22b, respectively. The control experiment curves of Figure 22 correspond to the 3DNEPH curves of Figure 19. In the control experiment, $\varepsilon_{LW} = 1.0$ for high clouds, as in *Wetherald and Manabe* [1980], i.e., the high clouds are assumed to be blackbody emitters. Also, the vertical placement of the clouds of Figure 1a,

the January 1977 standard cloud albedos of Table 1, and AFGWC observed snow cover are assumed.

Two of the longwave flux curves of Figure 22a correspond to extreme values of emissivity of high clouds, i.e., $\varepsilon_{LW} = 1.0$ and $\varepsilon_{LW} = 0.5$. However, the response varies rather linearly with ε_{LW} over this range. The high cloud tops in the control as well as in the $\varepsilon_{LW} = 0.5$ and $\varepsilon_{LW} = 1.0 + $ KTHERR experiments are as depicted in Figure 1a. In particular, within the 10°N to 0° latitude belt, they are located at level σ_4, where the vertical coordinate σ is the ratio of pressure to surface pressure and σ_4 denotes the model's fourth σ level, i.e., $\sigma_4 \sim 0.336$. But based upon aircraft measurements by *Appleman* [1961],
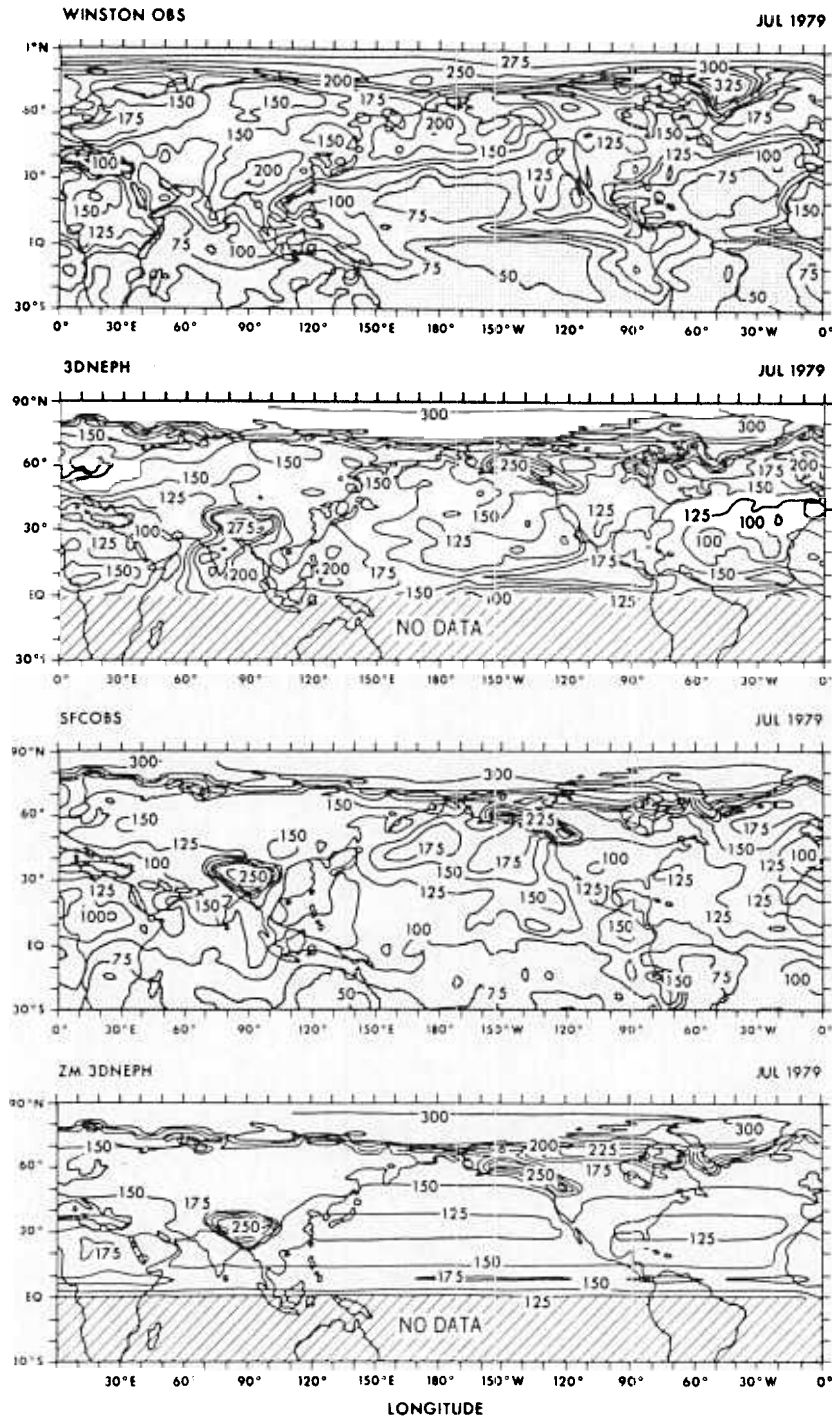
Fig 14b

the high cloud tops near the equator should be higher. Therefore, they were elevated to level $\sigma_3 \sim 0.189$ in experiment $\varepsilon_{LW} = 1.0 + KTH$. This modification caused the magnitude of ΔF to decrease for 3DNEPH clouds. Conversely, the bias increased at all latitudes (see curve $\varepsilon_{LW} = 1.0 + KTHERR$) when high clouds at sigma level σ_l $l = 3$ or $l = 4$ were lowered to level σ_{l+1}. This bias is comparable to that obtained when $\varepsilon_{LW} = 0.5$ or when an erroneous vertical temperature profile $T(\sigma_{l+1})$, $0.189 \leq \sigma_l \leq 0.500$, was inadvertently specified instead of $T(\sigma_l)$. Judging from Figure 9, the $T(\sigma_{l+1})$ profile corresponds to a temperature increase of ~ 15 K at high cloud top level.

The observed longwave flux profile could probably be reproduced by using different combinations of emissivity, cloud top height (or temperature), and amount of high clouds. The true values of these parameters are not precisely known. Nonetheless, if cloud top heights, cloud amounts, and emissivity corresponding to experiment $\varepsilon_{LW} = 1.0 + KTH$ are specified, then the best fit to $\Delta F = 0$ is obtained. Note that this specification of ε_{LW} is not consistent, though, with the emissivity–cloud albedo relationship of Stephens and Webster [1981] for high clouds.

Referring next to Figure 22b, the model-diagnosed zonal mean absored shortwave flux is rather biased in the control
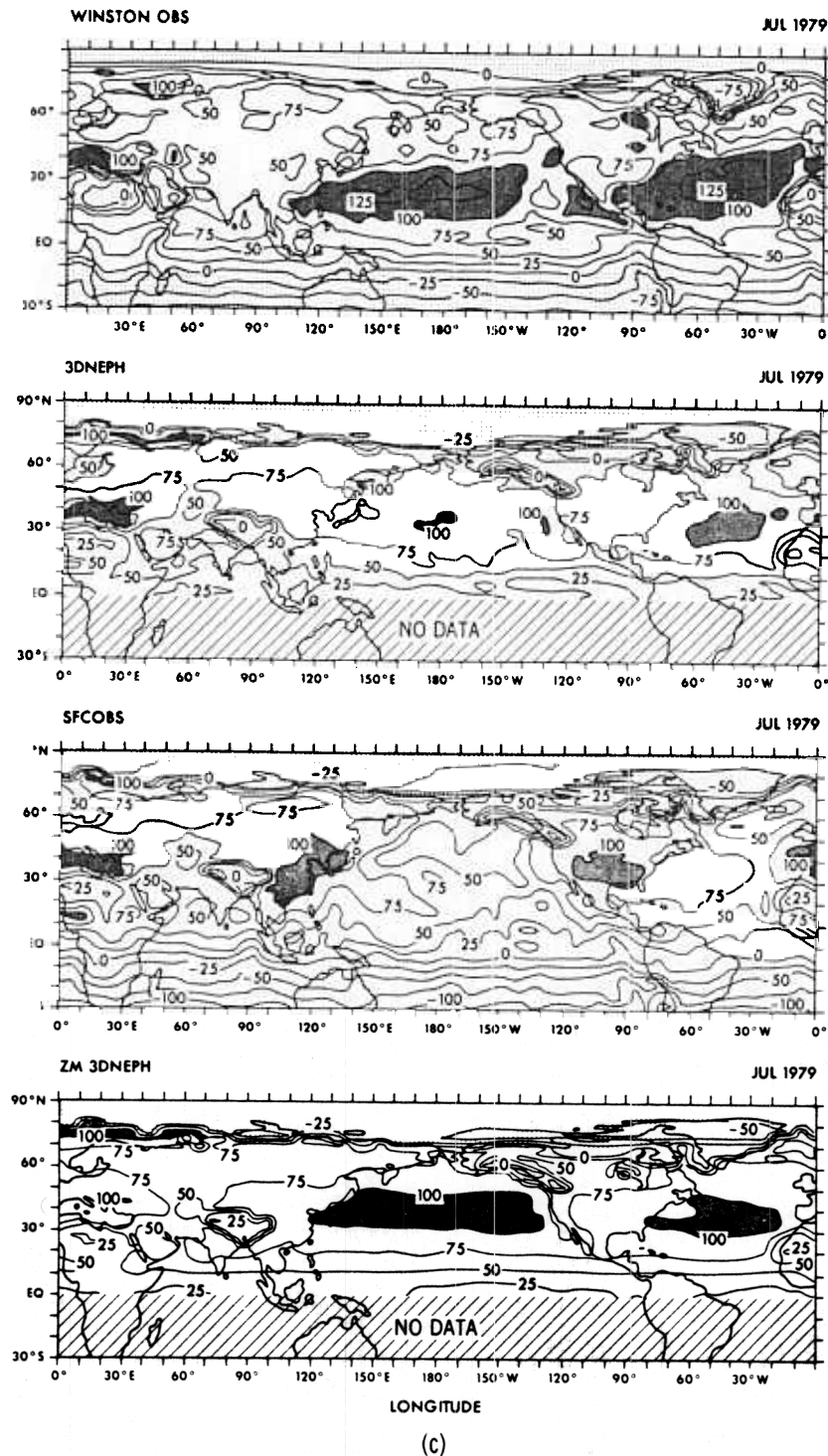
Fig. 14. Same as Fig. 13, except for July 1979 and the inclusion of (c) net radiative flux.

experiment. The standard specification of cloud albedos (see Table 1) used for this experiemnt was based upon *London* [1957]. However, more recent measurements, e.g., by *Drummond and Hickey* [1971], suggest that the albedos of low- and middle-level clouds, and especially their spectral reflectivities in the near infrared, should be lower. Also, cloud albedos appear to depend upon the zenith angle Z as discussed by *Wiscombe* [1975] and *Cess* [1976].

In any case, several experiments were carried out by using the "optional" cloud albedos or reflectivities and/or cloud ab-

sorptivities listed in Table 1. The cloud albedos were modified in one or more of the following ways: (1) their global mean values were reduced; (2) they were expressed as linear functions of cos Z; (3) different global mean reflectivities were specified for wavelengths $\lambda < 0.7$ μm vs. $\lambda \geq 0.7$ μm. The values adopted take into account the empirical findings discussed in *Drummond and Hickey* [1971] as well as *London* [1957]. They were used by *Wetherald and Manabe* [1980]. Concerning the second modification, the cos-Z-dependent formulae $A_i = \alpha_i + \beta_i \cos Z$, where $i = l$, m, or h, were adopted
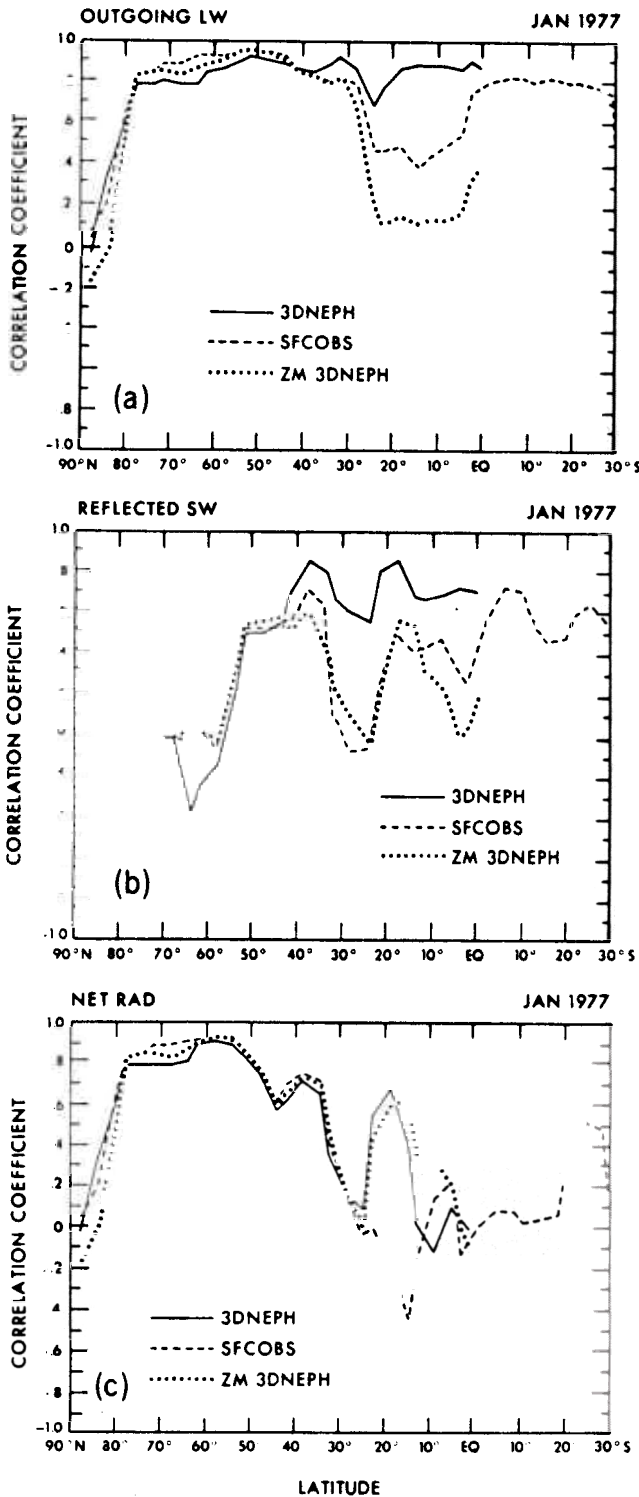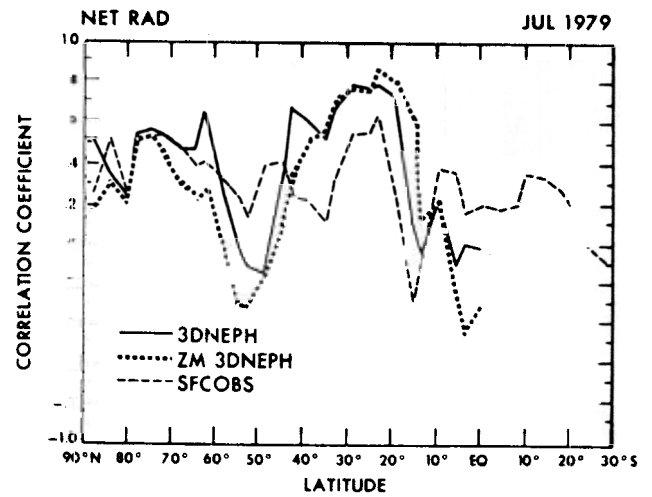
Fig. 16. Longitudinal correlation between model-diagnosed and observed net radiative flux vs. latitude for July 1979.

for $i = l, m, h$, where $\overline{\cos Z}$ is the global mean value of cos Z, and (2) a constraint on the relative amplitudes of β_h, β_m, and β_l, i.e.,

$$[\beta_j/\beta_l]\begin{Bmatrix}\text{option } b\\\text{option } d\end{Bmatrix} = [A_j/A_l]\begin{Bmatrix}\text{January 1977 standard case}\\\text{option } c\end{Bmatrix}$$

where $j = h$ or m.

The combination of modifications (1) and (2) produced the most dramatic improvement in model-diagnosed zonal mean absorbed shortwave flux for January 1977. The result for option b is indicated by the upper dashed curve of Figure 22b.

The absorbed shortwave flux biases for AFGWC observed snow cover (the control curve) vs. GFDL GCM climatological snow cover (lower dashed curve) are also compared in Figure 22b. The bias is slightly reduced in the 25°N–45°N latitude belt, given the observed snow cover.

Overall, the zonal mean longwave and shortwave flux differences are most sensitive to cloud top height and cloud albedo, respectively, for the range of parameters tested. Moreover, this sensitivity (Figure 22) is at least as great as the sensitivity to cloud amount (Figure 19). Also, the higher cloud top, modified

Fig. 15. Longitudinal correlation between model-diagnosed and observed radiative flux vs. latitude for January 1977: (a) outgoing longwave, (b) reflected shortwave and (c) net flux.

for the albedos of low, middle, and high clouds. They are rather ad hoc but were motivated by the discussion of Cess [1976]. The coefficients α_i and β_i (see Table 1) are determined from two constraints: (1) a global mean cloud albedo constraint

$$[\alpha_i + \beta_i \overline{\cos Z}]\begin{Bmatrix}\text{option } b\\\text{option } d\end{Bmatrix} = A_i\begin{Bmatrix}\text{option } a\\\text{option } c\end{Bmatrix}$$
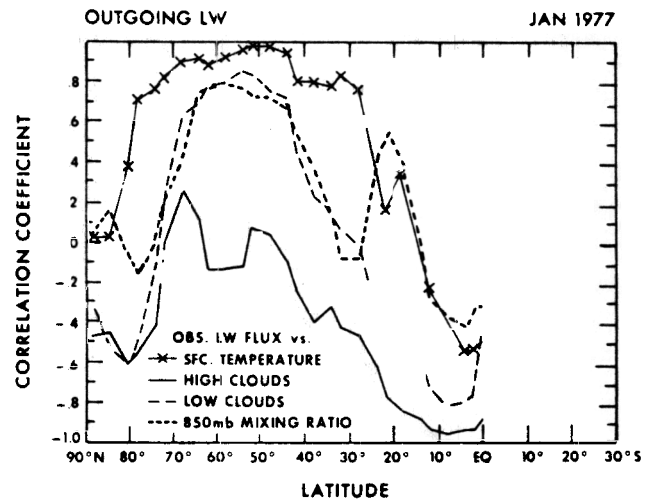

Fig. 17. Longitudinal correlation between selected meteorological variables and observed outgoing longwave flux vs. latitude. The case is January 1977, the clouds 3DNEPH, and the domain 90°N to 0°.
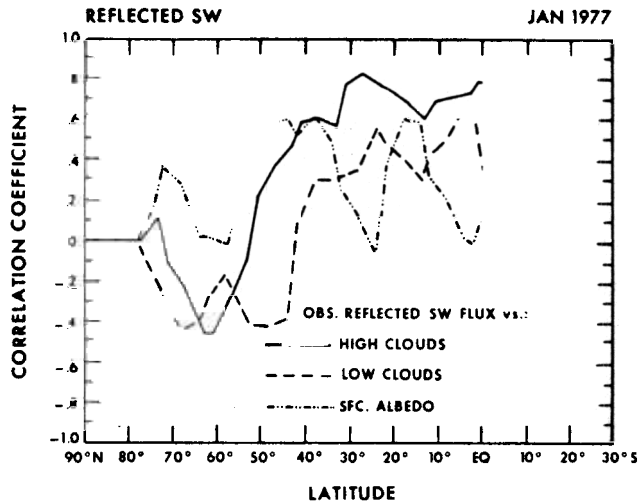
Fig. 18. Same as Fig. 17, except that the longitudinal correlation is between cloud amount or surface albedo and observed reflected shortwave flux.

cloud albedos, and, to a lesser extent, AFGWC snow cover act favorably on the biases of R (not shown). In fact the bias in the tropics does not exceed 20 W m^{-2} during January 1977 if modified cloud albedos and higher tops are incorporated simultaneously.

Figure 23 illustrates that the model-diagnosed $S\uparrow$ (and hence R) flux is more highly correlated with observation if the observed AFGWC snow cover is used instead of the GCM climatology. In contrast the cloud albedos are independent of longitude and have virtually no effect upon r_{St}. Likewise, use of $\varepsilon_{LW} \sim 0.5$ or the higher high cloud tops has little effect upon the correlation between model-diagnosed and observed F.

It is encouraging that values of cloud top height, cloud albedo, or snow cover that are presumably more realistic favorably affect model-diagnosed radiative fluxes. Of course, several more cases would have to be analyzed to establish statistical significance.

7. SUMMARY OF RESULTS AND CONCLUSIONS

Our investigation has focused upon three main topics:

1. Two monthly mean analyses of layered cloud amount, i.e., 3DNEPH and SFCOBS, were compared over the northern hemisphere domain for the months of January 1977 and July 1979. The data sources for the two analyses were quasi-independent. The 3DNEPH was constructed from the AFGWC 3D-Neph analysis, which incorporates satellite data as well as some surface observations and auxilliary meteorological data. In contrast, SFCOBS was based exclusively upon surface observations.

2. The sensitivity of radiative fluxes, especially at the top of the atmosphere, to the 3DNEPH and SFCOBS as well as zonal mean 3DNEPH monthly mean analyses of cloud amount was investigated. These radiative fluxes were diagnosed by the Fels-Schwarzkopf radiation model using monthly mean analyses of "observed" atmospheric temperature and water vapor data, and they were validated against NOAA 5 and TIROS-N satellite data.

3. The sensitivity of radiative fluxes at the top of the atmosphere to snow cover and to cloud parameters other than cloud amount was calculated. Here, 3DNEPH clouds were specified, while the temperature and water vapor fields and the radiation model were the same as in (2). The sensitivity calcu-

lations provided some indication of the relative importance of cloud amount vs. other radiative parameters for the model-diagnosed radiative balance. They also served as a check of some cloud-radiative parameterizations employed by the GFDL GCM.

The SFCOBS and 3DNEPH analyses of low cloud amount were in better agreement than the corresponding analyses of high cloud amount in the northern hemisphere winter extratropics. The SFCOBS analysis exhibited poorly defined ITCZ's, while the 3DNEPH July 1979 ITCZ was perhaps somewhat too intense.
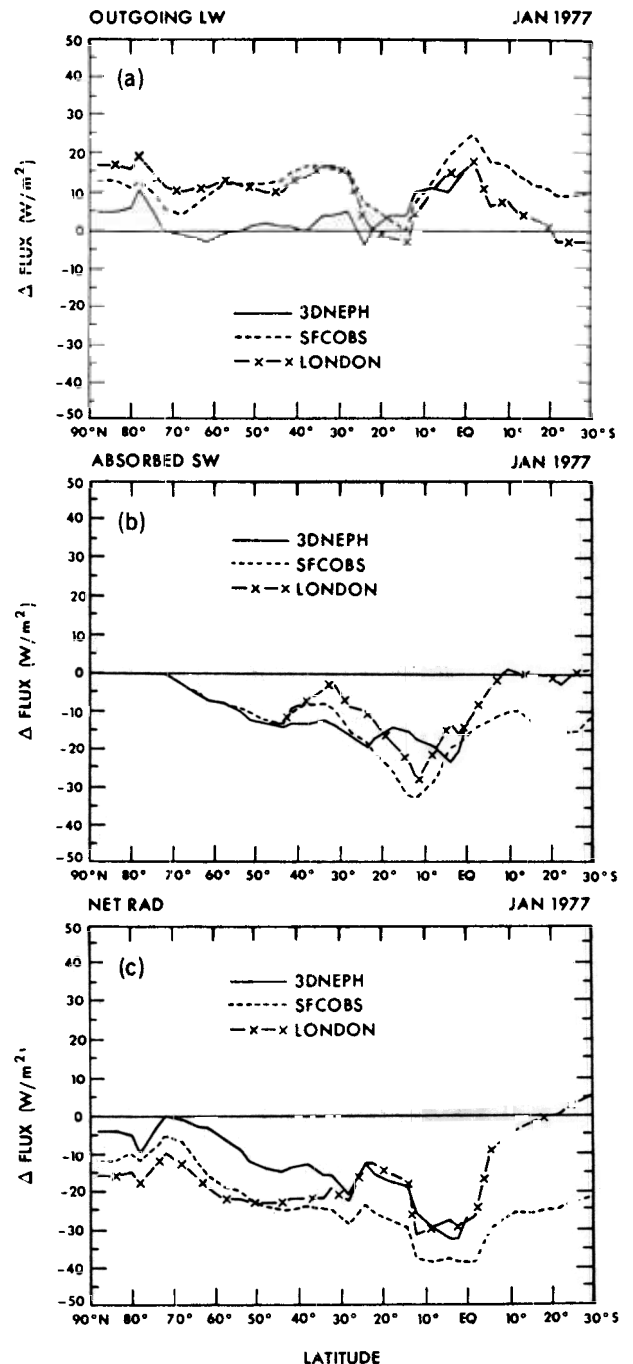

Fig. 19. Differential (i.e., model-diagnosed minus observed) zonal mean radiative flux vs. latitude for January 1977: (a) outgoing longwave, (b) absorbed shortwave, and (c) net radiative flux. Domain is 90°N–30°S. The units are W m^{-2}.

3DNEPH   JUL 1979

ZM 3DNEPH   JUL 1979
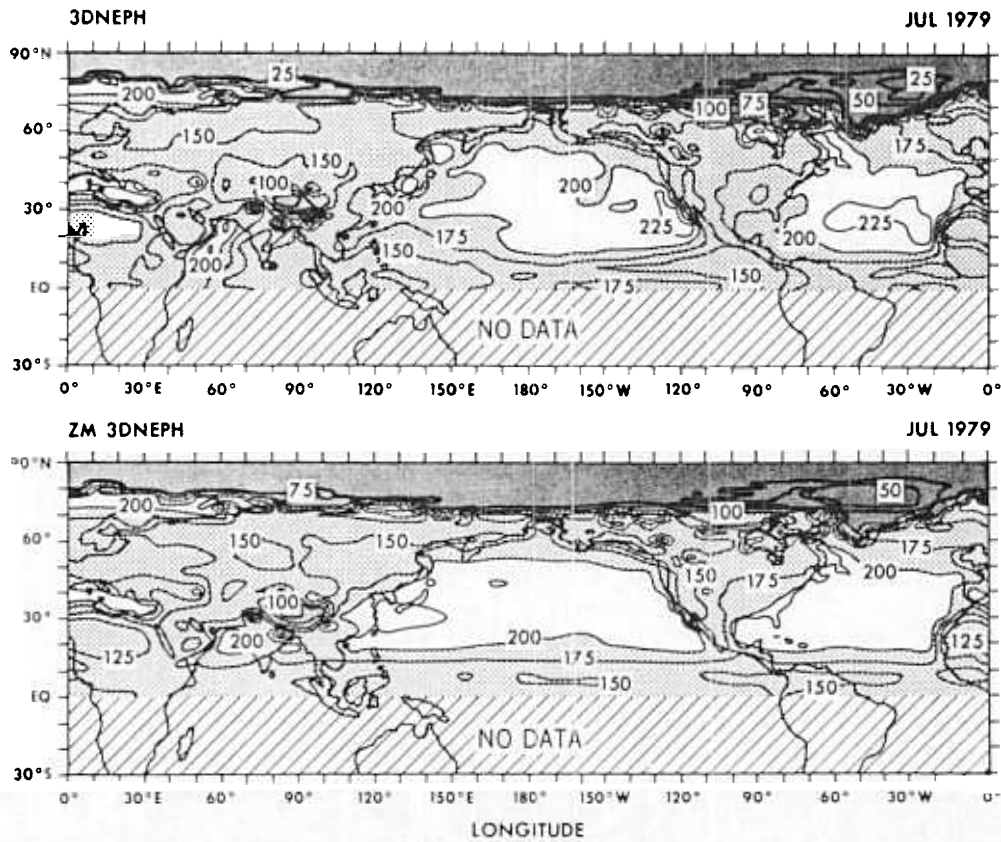
LONGITUDE

Fig. 20. Model-diagnosed fields of net radiative flux at the earth's surface for July 1979. Domain is 90 N–30 S. Contour interval is 25 W m⁻².

The model-diagnosed outgoing longwave flux F was very sensitive to the specification of cloudiness in the tropics. There, the longitudinal variation of F verified best for 3DNEPH clouds and poorly for SFCOBS and zonal mean 3DNEPH clouds. In the winter extratropics the surface temperature T_s exerted more influence than cloudiness. Nonetheless, F verified best in the extratropics over ocean as well as land, given 3DNEPH clouds. Meanwhile, the zonal mean bias ΔF was smaller at most latitudes for 3DNEPH (or zonal mean 3DNEPH) clouds than for SFCOBS clouds.

The model-diagnosed shortwave fluxes S bore less resemblance than F did to observation throughout the northern hemisphere. Unfortunately, the model-diagnosed net radiative

flux R correlated poorly with observation, whether SFCOBS or 3DNEPH cloudiness was specified. In fact there was virtually no improvement relative to zonal mean cloudiness. Also, in the July 1979 ITCZ the bias in model-diagnosed zonal mean shortwave flux was large and negative for 3DNEPH clouds compared to moderate and positive for SFCOBS (and LONDON) clouds. The 3DNEPH and SFCOBS net radiative fluxes both exhibited large negative biases in the tropics for different reasons, whereas the corresponding LONDON bias was fortuitously small.

Model-diagnosed fluxes at the earth's surface were calculated but were not verifiable. The net downward flux at the earth's surface was moderately sensitive to zonal mean vs.
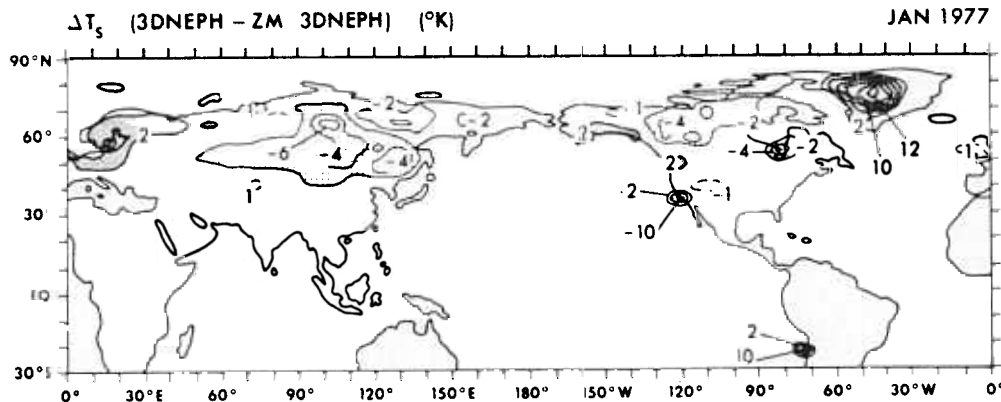
ΔT_s (3DNEPH – ZM 3DNEPH) (°K)   JAN 1977

Fig. 21. Surface temperature difference ΔT_s for January 1977, when zonal mean 3DNEPH clouds are replaced by longitudinally varying 3DNEPH clouds. The domain is 90°N–30°S. The ±1 K contours are dashed. In shaded or stippled regions the magnitude of the difference exceeds 2 K.

OUTGOING LW JAN 1977

(a)

$\epsilon_{LW} = 1.0$ (CONTROL)
$\epsilon_{LW} = 0.5$
$\epsilon_{LW} = 1.0 + $ KTHERR
$\epsilon_{LW} = 1.0 + $ KTH

ABSORBED SW JAN 1977

(b)

OBS. SNOW (CONTROL)
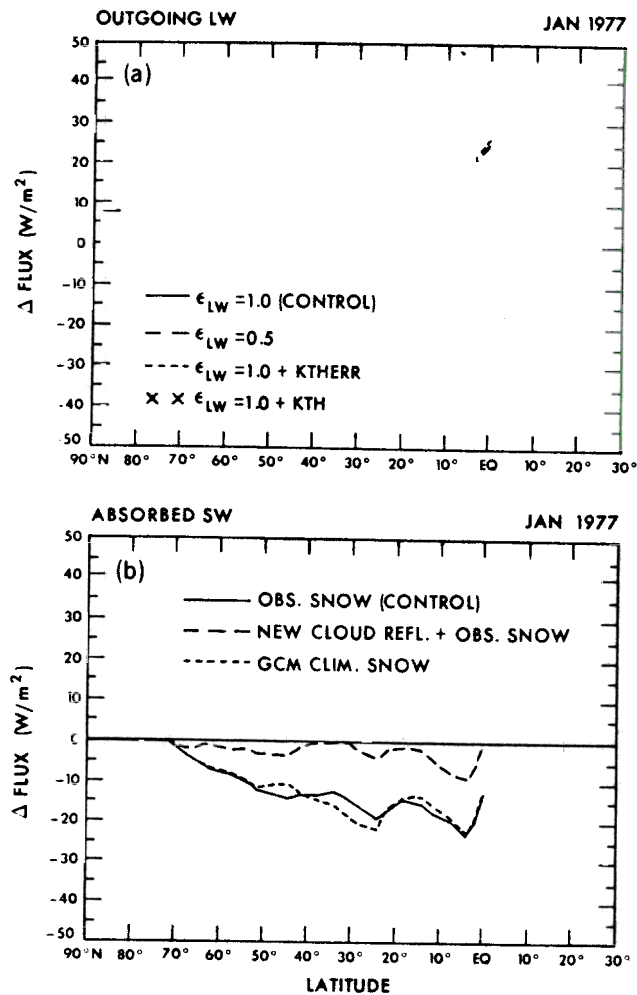NEW CLOUD REFL. + OBS. SNOW
GCM CLIM. SNOW

Fig. 22. Differential zonal mean radiative flux vs. latitude for different cloud-radiative parameterizations and snow depth fields: (a) longwave and (b) absorbed shortwave flux. The case is January 1977 and the domain 90 N to 0 . The units are W m^{-2}.

longitudinally varying 3DNEPH cloudiness. Most notably, a differential east-west gradient of 50 W m^{-2} was set up across the tropical Pacific Ocean in July 1979. Differences of $O(2$ K$)$ in model-computed surface temperature T_s over land in January 1977 were attributed to 3DNEPH vs. zonal mean 3DNEPH cloudiness.

Biases in the model-diagnosed zonal mean long- and shortwave radiative fluxes were reduced somewhat by adjusting the longwave emissivity of high clouds, tuning the vertical placement of the high cloud tops, and reducing the cloud albedos. The radiative flux biases were at least as sensitive to the latter two cloud parameters as to cloud amount. But those parameters hardly affected the longitudinal correlations between model-diagnosed vs. observed long- or shortwave fluxes. Conversely, use of an observed instead of a model-generated snow cover field yielded an improved correlation for $S\dagger$ while having only a small effect upon ΔS.

Conclusions

1. The 3DNEPH analysis of mean cloud amount for a particular month appears to have more longitudinal variation and to be more consistent with satellite-derived longwave flux data in the tropics than the SFCOBS analysis. This point may be reassuring to modelers who have avoided using the

AFGWC 3D-Neph on the grounds that it relies too much on bogus data and empirical relative humidity-cloudiness relationships.

2. Considering its satellite-oriented data base, a 3D-Neph climatology of low, middle, and high cloud amount would provide an interim benchmark for future satellite-derived cloud climatologies. Its establishment would be greatly facilitated by a drastically compressed data archive.

3. An improved scheme for calculating layered cloud amounts may still be needed, however, for climate and/or long-range forecast applications, where consistency between model-diagnosed vs. observed net radiative flux fields is essential. Constraints imposed on the longwave flux alone, as for example by the Meleshko and Wetherald [1981] scheme (see Appendix A), do not guarantee consistent net radiative fluxes. Preferably, the model-diagnosed shortwave as well as longwave fluxes and hence the net flux might be constrained to be consistent with satellite data.

4. Model-diagnosed calculations could perhaps be applied to other GCM forcing terms besides radiative fluxes. Accordingly, the relevant GCM diagnostics would be computed from observed (monthly) mean meteorological fields. By comparing those diagnostics against observation, biases of certain GCM parameters might be isolated. The above approach may be contrasted with the more traditional approach of making a series of costly long-term integrations, computing the bias of the GCM's time mean prediction, then trying to infer its possible causes(s).

Critique

The 3DNEPH analysis of layered cloud amount might be improved somewhat if the AFGWC-archived cloud-type information were utilized. Even more importantly, the AFGWC should archive cloud amounts of distinct cloud layers.

The SFCOBS analysis of layered cloud amount for individual months is inherently limited by huge data gaps over the oceans, tropics, and southern hemisphere. Perhaps the present scheme could be improved slighly by using the reported dominant cloud-type information to identify convective situations. For example, if cumulonimbus clouds were dominant and $N_T \sim n_l$, then the height of the low cloud top could be raised.

As previously noted, the contribution of transient eddy radi-

REFLECTED SW JAN 1977
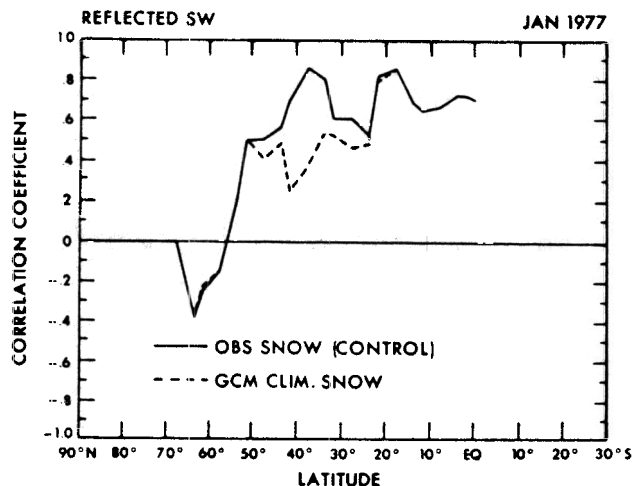
OBS SNOW (CONTROL)
GCM CLIM. SNOW

Fig. 23. Longitudinal correlation between model-diagnosed and observed reflected shortwave flux vs. latitude for two different snow cover specifications. The case is January 1977 and the domain 90°N

ative fluxes to the respective monthly mean fluxes was neglected. To assess the importance of this nonlinear effect for the radiative balance, model-diagnosed radiative fluxes could be calculated on a daily basis, then time averaged.

The values of certain cloud parameters in our GCM should be modified. Also, it would be desirable to utilize observed vertical temperature soundings to estimate cloud top heights, particularly if the vertical resolution of the GCM were refined. Finally, the recently completed CLIMAP surface albedo field is presumably more realistic than the *Posey and Clapp* [1964] specification.

APPENDIX A. MELESHKO ANALYSIS OF CLOUDINESS

Monthly mean analyses of low, middle, and high cloud amounts were generated for January 1977 and July 1979 over the $90°N-30°S$ latitudinal domain, using the scheme of *Meleshko and Wetherald* [1981]. These "Meleshko" analyses were excluded from the main text to simplify the comparison of the 3DNEPH vs. SFCOBS analyses. But they are of sufficient interest to warrant a brief discussion here.

As in *Meleshko and Wetherald* [1981] the layered cloud amounts are determined locally, given the values of the other cloud parameters, subject to three constraints:

1. The computed total cloud cover N_T for randomly overlapped cloud layers, i.e., $n_h + (1 - n_h)n_m + (1 - n_h)(1 - n_m)n_l$, is equal to the specified total cloud cover $N_{T_{obs}}$. The $N_{T_{obs}}$ field was provided by the 3DNEPH northern hemispheric and SFCOBS southern hemispheric monthly mean analyses of total cloud cover.

2. The ratios of cloud amount and of relative humidity h for the low vs. middle cloud layers are identical, i.e., $n_m/n_l = h_m/h_l$. This constraint had to be discarded at a few grid points to guarantee a physicaly realizable solution $0 < n_l, n_m, n_h < 1$.

3. The model-diagnosed outgoing longwave radiative flux at the top of the atmosphere is the same as the satellite-derived observation, i.e., "WINSTON OBS." Constraints 2 and 3 are simultaneously discarded and the fixup $n_l = N_{T_{obs}}$, $n_m = 0$, $n_h = 0$ imposed wherever the stratification is highly stable, e.g., over continents poleward of $40°N$ in January 1977.

The Meleshko analyses of n_l and n_h (not shown) are in best agreement with the 3DNEPH in the northern hemisphere tropics. There, the Meleshko n_h field, like the 3DNEPH, is strongly constrained by the longwave flux data, whereas the Meleshko N_T, and hence n_l, fields are constrained by the 3DNEPH $N_{T_{obs}}$. The Meleshko and 3DNEPH analyses of n_l for July 1979 bear some resemblance over the extratropical oceans. But over continental regions poleward of $40°N$ in January 1977, where the longwave constraint is ignored, the Meleshko analyses of n_h and n_l tend to be negatively correlated with the 3DNEPH. Meanwhile, in the southern hemisphere tropical oceans in January 1977, n_h is approximately consistent with the longwave flux observations. But since $N_{T_{obs}}$, which is based upon surface observations, is underestimated, so is n_l.

The Meleshko model-diagnosed radiative balance (not shown) is quite similar to the 3DNEPH. In particular, in the tropics and in the July 1979 northern hemisphere extratropics the Meleshko outgoing longwave flux verifies about equally well, and the Meleshko net radiative flux equally poorly, as the corresponding 3DNEPH fluxes. Thus a stronger radiative constraint than 3 is needed to generate model-diagnosed net fluxes at the top of the atmosphere that are consistent with observation.

APPENDIX B. BIASES IN THE OBSERVED SATELLITE DATA

Cess et al. [1982] have suggested that the NESDIS outgoing longwave fluxes are too insensitive to variations in cloud amount, whereas the absorbed shortwave fluxes are overly sensitive. The narrowness of the $10.5-12.5$ μm infrared channel and $0.5-0.7$ μm visible channel were cited as the two most important contributing factors. More recently, *Ohring et al.* [1984] have confirmed that the archived NOAA/NESS longwave fluxes possess a positive bias whose global mean is ~ 11 W m^{-2}. This flux-dependent bias is largest for low flux values, which occur with clouds of high, i.e., cold, cloud tops or cold surface temperatures. Ohring et al. attribute it to unrepresentative atmospheric temperature soundings used to develop regression relationships between the radiative flux vs. window radiance equivalent brightness temperatures. In other words the narrowness of the infrared window channel is not to blame per se. In any case we have recently applied the following correction formulas derived by A. Gruber (personal communication, 1984) to the longwave flux data on our GCM grid:

$$F = 0.792 \, F_{old} + 6.357 \times 10^{-4} \, F_{old}^2 \qquad (B1)$$

(January 1977)

$$F = 0.8154 \, F_{old} + 5.542 \times 10^{-4} \, F_{old}^2 \qquad (B2)$$

(July 1979), where F_{old} denotes the biased value and F the corrected value of longwave flux. To illustrate the variation of F with F_{old}, the January 1977 corrections for $F_{old} = 300$ W m^{-2} and 200 W m^{-2} are -6 W m^{-2} and -16 W m^{-2}, respectively. Only the WINSTON OBS F and R fields and the differential fluxes ΔF and ΔR were appreciably affected. Figures 13, 14, 19, and 22 were redrafted accordingly. Perhaps the most discernible change from the old results is that the magnitude of ΔF (see Figure 19a) becomes small for 3DNEPH clouds.

To help assess the impact of the width of the visible channel, we compared January 1977 3DNEPH model-diagnosed shortwave fluxes over the full visible near-infrared band vs. the $0.5-0.7$ μm band. In these calculations the cloud spectral reflectivities were assigned different values for wavelengths $\lambda < 0.7$ μm and > 0.7 μm, as in Table 1.

The correlation coefficient r_s, was insensitive to the full-band vs. narrow-band width. However, the full-band zonal mean model-diagnosed flux actually verified somewhat better in the tropics against the NOAA 5 satellite data than did its narrow-band counterpart. We then discovered that the sensors aboard NOAA 5 have half-width response limits of ~ 0.5 and 0.93 μm. Unfortunately, the flux contribution over this broader band cannot be readily isolated in the Fels-Schwarzkopf radiation model. Also, the wavelength dependence of the surface albedo was not taken into account. With these caveats, the narrowness of the NOAA 5 shortwave channel was apparently not detrimental to our results.

As *Cess et al.* [1982] have noted, the infrequent, i.e., one pass per day sampling in the visible channel, may yield planetary albedos that are unrepresentative of the diurnal mean. In principle the NOAA measurement could be augmented by two DMSP measurements, when two DMSP satellites are in orbit, as in July 1979. But the DMSP radiative fluxes have not been archived by the AFGWC.

lar. Also, S. Manabe, D. S. Schwarzkopf, and R. T. Wetherald kindly reviewed the manuscript and offered numerous valuable suggestions. The manuscript was typed by Betty Williams. The figures were drafted by P. Tunison and W. Ellis and photographed by J. Conner.

REFERENCES

Appleman, H. S., Occurrence and forecasting of cirrostratus clouds, *Tech. Note 39*, World Meteorol. Org., Geneva, 1961.

Berlyand, T. G., and C. A. Strokina, Cloudiness regime over the globe (in Russian), *Tr. Gl. Geofiz. Obs.*, *338*, 3–20, 1974.

Bignell, K. J., The water-vapor infra-red continuum. *Q. J. R. Meteorol. Soc.*, *96*, 390–403, 1970.

Cess, R. D., Climate change: An appraisal of atmospheric feedback mechanisms employing zonal climatology, *J. Atmos. Sci.*, *33*, 1831–1843, 1976.

Cess, R. D., B. P. Briegleb, and M. S. Lian, Low-latitude cloud amount and climate feedback: Comparative estimates from satellite data. *J. Atmos. Sci.*, *39*, 53–59, 1982.

Clapp, P. F., Global cloud cover for seasons using TIROS nephanalyses, *Mon. Weather Rev.*, *92*, 495–507, 1964.

Drummond, A. J., and J. R. Hickey, Large-scale reflection and absorption of solar radiation by clouds as influencing earth radiation budgets: New aircraft measurements, paper presented at International Conference on Weather Modification, Am. Meteorol. Soc., Canberra, 1971.

Fels, S. B., and M. D. Schwarzkopf, The simplified exchange approximation, A new method for radiative transfer calculations, *J. Atmos. Sci.*, *32*, 1475–1488, 1975.

Fels, S. B., and M. D. Schwarzkopf, An efficient, accurate algorithm for calculating CO_2 15-μm band cooling rates, *J. Geophys. Res.*, *86*(C2), 1205–1232, 1981.

Fye, F. K., The AFGWC automated cloud analysis model, *Tech. Memo. 78-002*, 97 pp., Air Force Golbal Weather Central, Offut Air Force Base, Nebr., 1978.

Gordon, C. T., and W. F. Stern, A description of the GFDL global spectral model, *Mon. Weather Rev.*, *110*, 625–644, 1982.

Gruber, A., Determination of the earth-atmosphere radiation budget from NOAA satellite data, *NOAA Tech. Rep. NESS 76*, Nat. Environ. Sat. Serv., Wash., D. C., 1978.

Hartmann, D. L., and D. A. Short, On the use of earth radiation budget statistics for studies of clouds and climate, *J. Atmos. Sci.*, *37*, 1233–1250, 1980.

Henderson-Sellers, A., N. A. Hughes, and M. Wilson, Cloud cover archiving on a global scale, A discussion of principles, *Bull. Am. Meteorol. Soc.*, *62*, 1300–1307, 1981.

Hering, W. S., and T. R. Borden, Jr., Mean distribution of ozone density over North America, 1963–1964, Environmental Research Papers, *Rep. 162*, U.S. Air Force Cambridge Res. Lab., Hansom Field, Mass., 1965.

Hoyt, D. V., Percent of possible sunshine and the total cloud cover, *Mon. Weather Rev.*, *105*, 648–652, 1977.

JOC/Report of the JOC Study Conference on Parameterization of Extended Cloudiness and Radiation for climate Models, World Meterol. Org., Oxford, England, Sept. 27–Oct. 4, 1978.

Lacis, A. A., and J. E. Hansen, A parameterization for the absorption of solar radiation in the earth's atmosphere, *J. Atmos. Sci.*, *31*, 118–132, 1974.

Landsberg, H., Climatology, in *Handbook of Meteorology*, edited by F. A. Berry, Jr., E. Bollary, and N. R. Beers, Section 12, pp. 928–997, McGraw-Hill, New York, 1945.

Levitus, S., and A. H. Oort, Global analysis of oceanographic data, *Bull. Am. Meteorol. Soc.*, *58*, 1270–1284, 1977.

London, J., A study of the atmospheric heat balance, Final Report, *AFCRC Contract AF 19(122)-165*, 99 pp., N.Y. Univ., New York, 1957.

London, J., Mesospheric dynamics, 3, The distribution of total ozone in the northern hemisphere, Final Report, Dep. Meteorol. Oceanogr., N.Y. Univ., New York, 1962.

Meleshko, V. P., and R. T. Wetherald, The effect of a geographical cloud distribution on climate: A numerical experiment with an atmosphere general circulation model, *J. Geophys. Res.*, *86*(C12), 11,995–12,014, 1981.

Mellor, G. L., and T. Yamada, A hierarchy of turbulence closure models for planetary boundary layers, *J. Atmos. Sci.*, *31*, 1791–1806, 1974.

Miyakoda, K., C. T. Gordon, R. Caverly, W. Stern, J. Sirutis, and W. Bourke, Simulation of a blocking event in January 1977, *Mon. Weather Rev.*, *111*, 846–869, 1983.

Ohring, G., and P. Clapp, The effect of changes in cloud amount on the net radiation at the top of the atmosphere, *J. Atmos. Sci.*, *37*, 447–454, 1980.

Ohring, G., A. Gruber, and R. G. Ellingson, Satellite determination of the relationship between total longwave radiation flux and infrared window radiance, *J. Appl. Meteorol.*, in press, 1984.

Payne, R. E., Albedo of the sea surface, *J. Atmos. Sci.*, *29*, 959–970, 1972.

Ploshay, J. J., R. K. White, and K. Miyakoda, FGGE level III-B daily global analyses, Part 1, *NOAA Data Rep ERL GFDL-1*, Geophys. Fluid Dyn. Lab., Princeton, N. J., 1983.

Posey, M. W., and P. F. Clapp, Global distributions of normal surface albedo, *Geofis. Int.*, *4*(1), 33–48, 1964.

Rosen, R. D., and D. A. Salstein, A comparison between circulation statistics computed from conventional data and NMC Hough analyses, *Mon. Weather Rev.*, *108*, 1226–1247, 1980.

Sadler, J. C., L. Oda, and B. J. Kilonsky, Pacific ocean cloudiness from satellite observations, *Tech. Rep. UHMET 76-01*, Dep. Meteorol., Univ. Hawaii, Honolulu, 1976.

Sasamori, T., J. London, and D. V. Hoyt, Radiation budget of southern hemisphere, in *Meteorology of the Southern Hemisphere, Meteorol. Monogr. 13*, edited by C. W. Newton, American Meteorological Society, Boston, 1972.

Schneider, S. H., Cloudiness as a global climatic feedback mechanism: The effects on the radiation balance and surface temperature of variations in cloudiness, *J. Atmos. Sci.*, *29*, 1413–1422, 1972.

Stephens, G. L., and P. J. Webster, Sensitivity of radiative forcing to variable cloud and moisture, *J. Atmos. Sci.*, *36*, 1542–1556, 1979.

Stephens, G. L., and P. J. Webster, Clouds and climate: Sensitivity of simple systems, *J. Atmos. Sci.*, *38*, 235–247, 1981.

Telegadas, K., and J. London, A physical model of the northern hemisphere troposphere for winter and summer, *Sci. Rep. 1, Contract AF 19(122)-165*, 55 pp., Res. Div., Coll. Eng., N.Y. Univ., New York, 1954.

Warren, S. G., C. Hahn, and J. London, Ground-based observations of cloudiness for cross-validation of satellite observations, paper presented at workshop on Clouds in Climate: Modeling and Satellite Observational Studies, Oct. 29–31, 1980, NASA Goddard Inst. Space Stud., New York, 1981.

Wetherald, R. T., and S. Manabe, Cloud cover and climate sensitivity, *J. Atmos. Sci.*, *37*, 1485–1512, 1980.

Wiscombe, W. J., Solar radiation calculations for summer stratus conditions, in *Climate of the Arctic*, edited by G. Weller and S. A. Bowling, Geophysical Institute, University of Alaska, Fairbanks, 1975.

C. T. Gordon, R. D. Hovanec, and W. F. Stern, Geophysical Fluid Dynamics Laboratory/NOAA, Princeton University, Princeton, NJ 08540.